

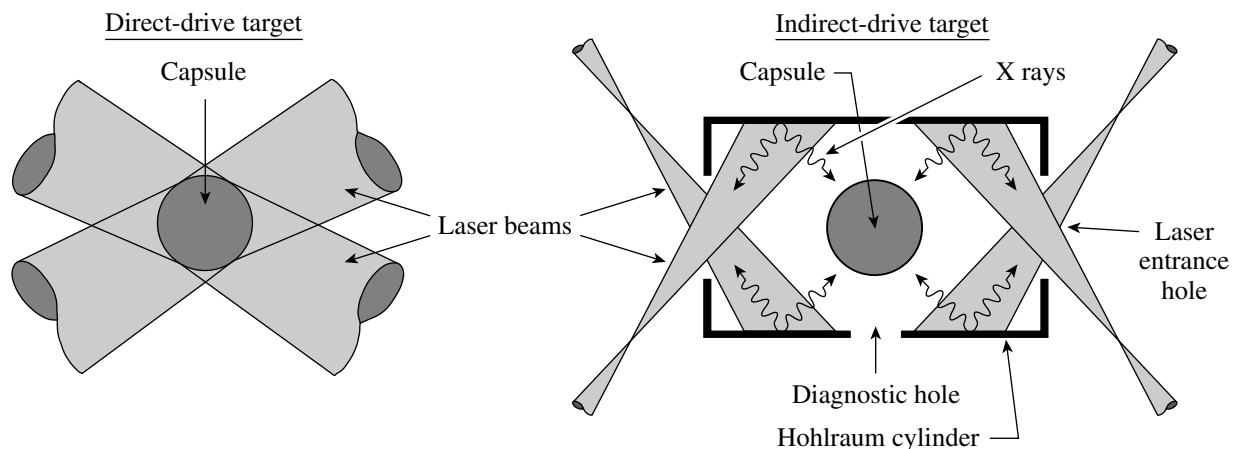
## 2. OMEGA Laser System

### 2.1 OMEGA 60-BEAM COMPRESSION FACILITY

#### 2.1.1 Introduction

This section describes the design\* of the OMEGA Laser System and summarizes the operation. A complete description of the system can be found at [www.lle.rochester.edu](http://www.lle.rochester.edu). An upgrade project undertaken from October 1990 to May 1995 consisted of a complete overhaul of the building housing the Omega Laser Facility. Prior to the upgrade, OMEGA was a 24-beam, 2-kJ, 351-nm laser. OMEGA now has 60 beams and can deliver up to 30 kJ of 351-nm laser energy. The upgrade took 4.5 yr and \$61M to complete. The OMEGA Laser System provides a unique capability to validate high-performance, direct-drive laser-fusion targets. The ultimate goal of the Laboratory for Laser Energetics (LLE) experimental program on OMEGA is to study the physics of hot-spot formation under near-ignition conditions (ignition scaling), using cryogenic targets whose hydrodynamic behavior scales to that of high-gain targets.

Many key physics issues associated with capsule implosions are common to both direct and indirect drive. Studies of drive uniformity, hydrodynamic instabilities, and energy coupling to the capsule are relevant to either approach. [Direct and indirect drive refer to the way the laser couples to the target (see Fig. 2.1)]. The Omega Laser Facility is central to developing platforms (laser conditions, diagnostic configurations, and target systems) for later use at the National Ignition Facility (NIF).



Key physics issues addressed  
by experiments on OMEGA

- Energy coupling
- Drive uniformity
- Hydrodynamic instabilities

E6426bJ1

Figure 2.1

Direct-drive targets are driven by laser irradiation that impinges directly on the capsule. Indirect-drive targets are compressed by x rays generated when the laser impinges on a cylindrical “hohlraum” that surrounds the target.

\*The detailed configuration of the Omega Laser Facility is evolving as new capabilities and improvements are implemented. The user is advised to consult with the OMEGA or OMEGA EP Facility Manager regarding any detailed system specifications and experimental requirements prior to the detailed design of an experiment.

## 2.2 SYSTEM DESCRIPTION

### 2.2.1 System Performance

The system is installed in the space previously occupied by the 24-beam OMEGA laser and capitalizes on the experience gained over three decades of system operations. The uniformity, total-energy, and pulse-shaping requirements for the ignition-scaling experiments established the operational performance envelope of the 60-beam system. It can produce 30 kJ on target in temporally shaped pulses with peak powers of up to 30 TW. The top-level performances routinely achieved are given in Table 2.1.

Table 2.1: OMEGA specifications.

Energy on target	Up to 30 kJ in a 1-ns square pulse
Wavelength	351 nm (third harmonic of Nd:glass)
Lasing medium	Nd-doped phosphate glass
Number of beams	60
Irradiation nonuniformity	1% to 2%
Beam-to-beam energy balance	Less than 4% rms on target
Beam-to-beam power balance	<1% at peak
Beam smoothing	<ul style="list-style-type: none"> <li>• Spectral dispersion</li> <li>• Polarization smoothing</li> <li>• Phase smoothing</li> </ul>
Pulse shaping	0.1- to 4-ns arbitrary shapes with 40:1 contrast
Repetition rate	One shot/h nominal; one shot/45-min max rate
Laser and diagnostic pointing	Any location within 1 cm of target chamber center

The on-target energy is dictated by the requirement to conduct hydrodynamically equivalent capsule implosions that produce diagnostic signatures sufficient to adequately diagnose the fuel-core performance. Short-wavelength (351-nm) ultraviolet laser light has long been attractive as a laser-fusion driver because of its enhanced absorption and reduced hot-electron production. The Nd:glass master-oscillator/power amplifier system produces 60 beams of infrared energy (1054 nm). Each beam is converted to the ultraviolet at the end of the amplifiers prior to being delivered to the target. The optical assembly that performs this conversion is referred to as the frequency-conversion crystal (FCC) subsystem. OMEGA uses two UV high reflectors after frequency conversion to separate the drive energy from the unconverted light prior to focusing the beams on target.

The uniformity of the laser has two parts: (1) each beam produces a uniform spot on target and (2) the beam-to-beam power variation on target is kept to a minimum. On-target uniformity benefits from the 60-beam configuration because the power delivered to any given point on a spherical target is derived from many beams. As a result of the beams overlapping on target, a beam-to-beam energy balance of 3% to 4% is sufficient to produce an on-target irradiation uniformity of 1% to 2%. Power balance is achieved by ensuring that the time history of the energy's arrival at the target is the same

for each beam. This is achieved by minimizing the beam-to-beam variation of the gain produced by each amplification stage and by equalizing the time of arrival on target.

The instantaneous uniformity of the energy within a given beam spot on the target is optimized by applying the three beam-smoothing techniques listed in Table 2.1. Phase smoothing is provided by distributed phase plates (DPP's) inserted in each beam that essentially "break up" the individual beams into several thousand beamlets on target. Smoothing by spectral dispersion (SSD) is a technique that modulates the wavelength of the master-oscillator pulse. This causes the speckle points within the on-target spot to move during the period of irradiation. Polarization smoothing is achieved by passing the UV beam through a distributed phase rotator (DPR) optic as it propagates to the target. The DPR splits each beam into two orthogonally polarized (non-interfering) beams with a small pointing offset. Overlapping of the spots of the two polarizations has a time-instantaneous beam-smoothing effect.

A versatile capability to produce temporally shaped pulses is also employed to minimize hydrodynamic instabilities in the implosions.

The nominal system repetition rate of one shot per hour facilitates a productive experimental program.

### 2.2.2 Laser-Energy Performance

A variety of ultraviolet (UV) pulse shapes that tailor the target drive for a specific experiment are available. While the infrared (IR) performance is relatively independent of the pulse shape, UV power is strongly dependent on shape because the conversion to UV is a nonlinear, intensity-dependent process. The system performs nearly optimally with a 1-ns square pulse, which is to say that maximum UV energy can be delivered to the target with a 1-ns square pulse. An arbitrary waveform generator can generate a PI specified shape if there are unique drive requirements for an experiment. Any unique shapes must be specified well in advance of an experiment to allow for design, analysis, and test time. The format of the Pulse-Shape Request is described in the Pulse-Shape Request web page on the Omega Operations web page, and is typically a simple excel file that allows the PI to request desired power versus time.

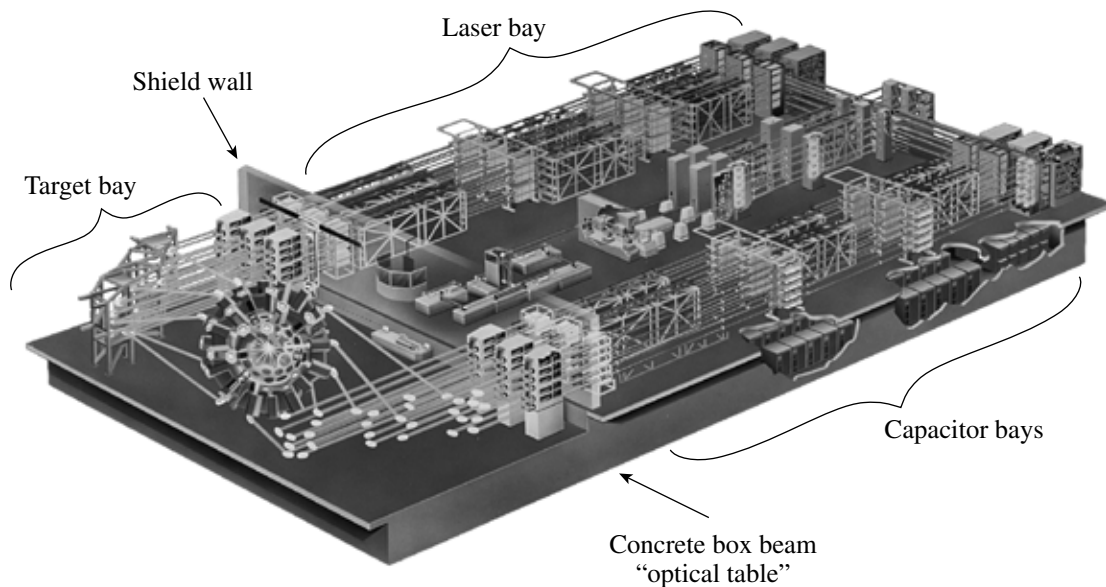
The overall energy performance predicted for a 1.0-ns square pulse on OMEGA is shown in Table 2.2. This table outlines the performance for the cases of no-SSD bandwidth and for 1.0-THz-SSD bandwidth at nominal system peak power and with the best IR- to UV-conversion setting. The energies quoted are summed over the 60 beams and reflect 0.84-kJ IR per beam prior to conversion. The UV on-target numbers include a 4.1% loss at the UV diagnostic pickoff and an additional 8% loss resulting from the transport system, including transport mirrors, DPR's, DPP's, focus lenses, vacuum windows, and debris shields. The average fluence is the maximum average fluence in the pulse including the effects of gain saturation and the radially varying gain profile of the system. The peak fluence is taken as  $1.78\times$  the maximum average fluence based on experience at LLE and elsewhere. Although FCC's have been upgraded to enhance broad-bandwidth frequency-conversion efficiency, there is nearly a 25% energy penalty for 1-THz operation.

Table 2.2: Energy performance of OMEGA with a 1.0-ns square pulse.

	No SSD bandwidth	0.33-THz SSD
Peak power of main pulse (TW)	30 TW	27 TW
UV energy on target (kJ)	30	27

### 2.2.3 Top-Level Configuration

The 60-beam OMEGA Laser System is installed in the same facility that formerly housed the 24-beam OMEGA system. A significant feature of the facility is the concrete box beam structure (67 m long, 29 m wide, and 4.9 m high) that serves as an “optical table” on which the laser is built. This optical table rests on a bed of gravel and is structurally independent from the laboratory building enclosing it. As shown in Fig. 2.2, the OMEGA Laser System is installed on the optical table in two bays, separated by a neutron-absorbing shield wall. The shield wall includes a viewing area called the “Visitors’ Gallery,” which looks into both bays. The western bay contains the IR laser components and is called the Laser Bay. The eastern bay is dominated by the target mirror structure (TMS) and target chamber (TC) and is called the Target Bay. The Laser Bay and Target Bay are climate controlled and designed to operate as Class-1000 clean rooms, but actually perform to nearly Class-100 conditions by limiting access and sources of contamination that come from personnel activity. The area inside the facility below the Laser Bay contains the capacitor bays, which house the power conditioning system that powers the laser amplifiers. The Pulse Generation Room (PGR) is also below the Laser Bay. The area below the Target Bay, called LaCave, contains support systems for experimental diagnostics and the target insertion portion of the Cryogenic Target Handling System



TC2998J1

Figure 2.2  
The OMEGA Laser System is built on a concrete structure that is independent of the surrounding building.

(CTHS). Supporting systems, such as the laser spatial-filter vacuum piping, deionized (DI)/glycol cooling piping, and nitrogen gas piping, are also installed beneath the Laser Bay. The Control Room is located in the laboratory building just north of the Laser/Target Bays. The laboratory building also houses offices, laboratories, and supporting services.

Figure 2.3 is a schematic representation of the elements that make up the OMEGA Laser System. Figure 2.4 illustrates the physical layout of the same elements. The laser drivers subsystem produces the shaped seed pulses and delivers them to the stage-A splitter in the Laser Bay. The remainder of the beam-handling equipment, up to the target itself, is referred to as the optomechanical subsystem. It includes the laser optical system and six power-amplifier stages. These components amplify the pulses, divide them into 60 beams, and control arrival time at the target, energy, polarization, and spatial distribution of each beam. The optomechanical system also includes the frequency-conversion crystals and Target Bay subsystems, which transport the beams to the target, and align and focus them precisely. The experimental system includes the target subsystems, which establish and maintain a vacuum within the target chamber and insert and position the targets, and the experimental diagnostic instruments that acquire data during shots.

The laser beams originate in the Driver Electronic Room (DER) located below the laser driver area in the Laser Bay. The shaped pulses produced in the DER are sent via optical fiber to the PGR, which is located adjacent to the DER. The PGR is the facility where the laser beam is spatially formed and, in the case of the SSD driver, modified substantially to improve the on-target laser uniformity. The driver beams go through a periscope to the laser bay where they are distributed to two separate amplifier systems: (1) the SSD and (2) the backlighter large-aperture ring amplifiers (LARA's). After amplification in the LARA, each beam is spatially filtered and propagates west into the stage-A beam splitter. As is detailed in the next section, these two sources can be configured to produce a variety of target-irradiation conditions.

The single driver beam is split three ways at the A-split; at this split there is an option to feed one leg of the three-way split with the backlighter driver. The backlighter driver can feed any one of the three legs with an independent timing and pulse shape. The leg that is fed by the backlighter then goes to one third of OMEGA (20 beams). All the beam splitters are configured with polarization-control wave plates that provide the ability to accurately control the energy balance between beams. After the A-split, each beam is amplified and split five ways (B-split), resulting in 15 beams. These beams, now at one fifth the output energy of the A amplifiers, are amplified again. The stage-A and stage-B amplifiers are 64-mm rod amplifiers. The 15 beams are then expanded and propagated through 90-mm amplifiers (stage C).

Each beam is then split four ways at the end of the bay. The resulting 60 beams pass through assemblies that permit path-length adjustment needed to compensate for unavoidable differences in transport paths to the target chamber or to provide precision beam-timing delay for experiments. This adjustment makes it possible to control individual beam arrival times to ~10 ps. The 9-ns travel range available on each beam permits intentional mistiming of beams for special experimental configurations.

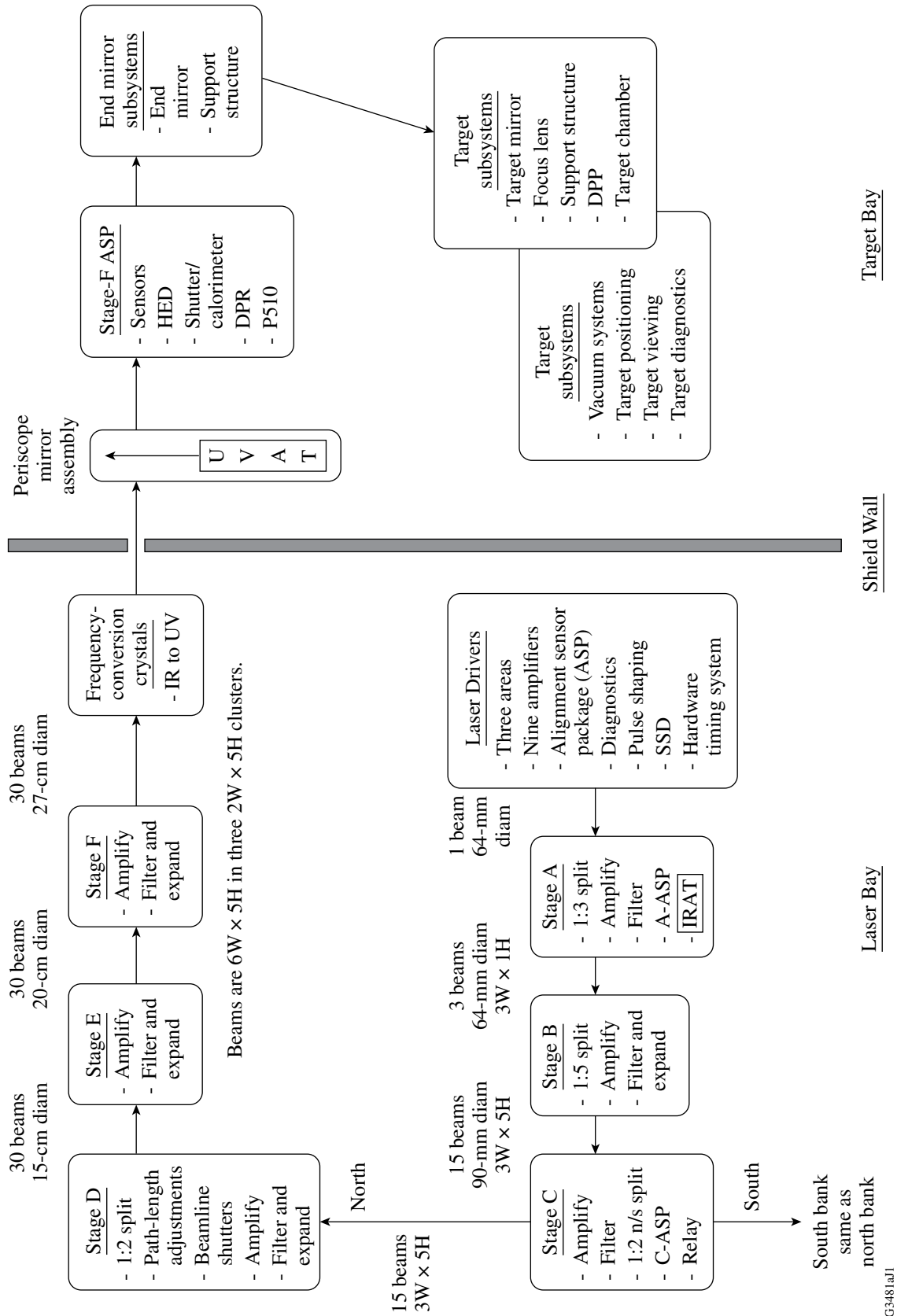


Figure 2.3  
A schematic of OMEGA. IRAT and UVAT are the IR and UV alignment tables; ASP's are alignment sensor packages.

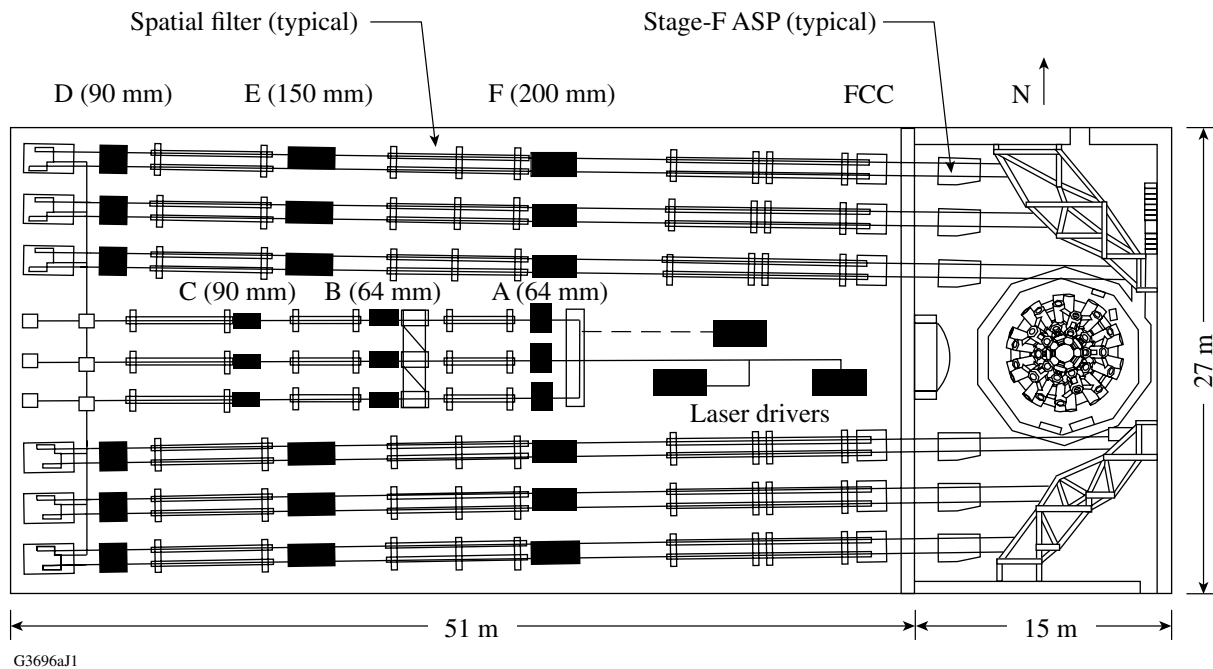


Figure 2.4

The physical layout of OMEGA. The location of four stages of rod amplifiers (A–D), two stages of disk amplifiers (E, F), and the frequency-conversion crystals (FCC’s) are indicated.

The 60 beams then propagate eastward, back down the length of the Laser Bay: 30 beams on the north side and 30 beams on the south side. The beams are arrayed in six clusters of ten beams (two wide, five high). Each beam passes through a second 90-mm rod amplifier (stage D) before being amplified by the stage-E and stage-F disk amplifiers. (These feature clear-aperture diameters of 150 mm and 200 mm, respectively.) Both the 64-mm and 90-mm rod amplifiers are modified versions of the original OMEGA amplifiers and are pumped by 12 longitudinal flash lamps along the barrel of the rod. In the disk amplifiers, the laser gain media is a face-pumped disk geometry because rod amplifiers are not feasible at the larger apertures. The disk amplifiers are termed single-segment amplifiers, or SSA’s, because each amplifier is dedicated to a single beam.

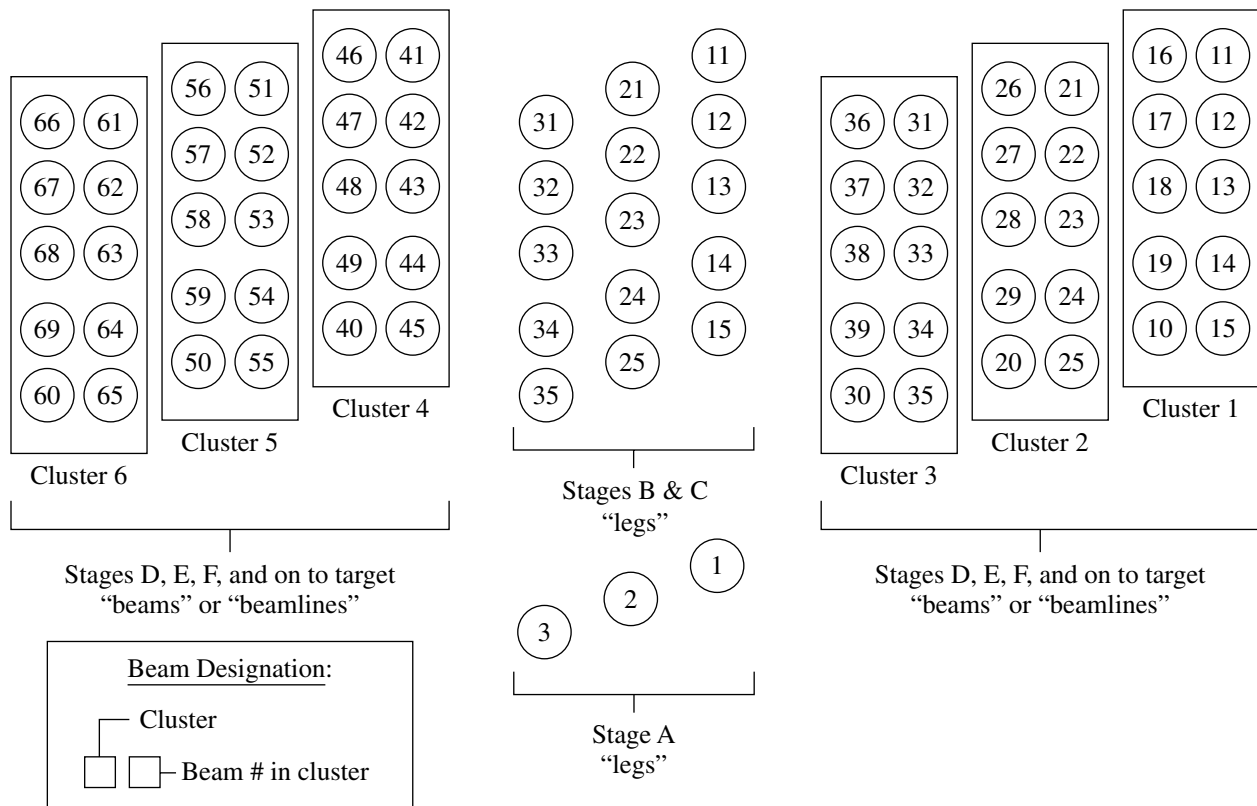
The 30 beams propagating toward the Target Bay on each side of the Laser Bay are all mutually parallel but are angled  $0.75^\circ$  toward the center of the Laser Bay. This angle is required to map the 60 beams onto the spherical target chamber using only two mirrors per beam while limiting the incident angle on the mirrors to  $60^\circ$  or less. Additional advantages of this wedged configuration are that it minimizes the in-air path length of the UV transport system to a total of 18-m propagation in air. Minimization of in-air path length is required to stay below the thresholds where stimulated rotational Raman scattering (SRRS) will occur. SRRS is a phenomenon that can degrade the performance of the system and/or damage transport optics.

At each stage of the laser, spatial filtering is used to remove high-spatial-frequency noise in the beam and to ensure correct image relaying. Image relaying is critical to the performance of

laser beams with SSD because it prevents excessive excursions of different frequencies across the beam aperture. Spatial filtering mitigates the beam degradation that would otherwise result from the frequency-dependent, grating-induced differences in propagation directions. Image relaying and spatial filtering also prevent intensity modulation caused by interference effects and nonlinear, intensity-dependent phase errors.

The power-amplified beams are spatially filtered and magnified to a clear aperture of 280 mm. They then propagate through thin-film polarizers before reaching the FCC's. The polarizers maximize conversion efficiency by ensuring that the correct linear polarization is incident upon the crystals. UV light reflected from the target is prevented from propagating backward through the laser system by a UV-absorbing window on the input of the frequency-conversion cells. Frequency conversion to the third harmonic (351 nm) is carried out using the polarization-mismatch method developed at LLE. After frequency conversion, the beams pass through holes in the 76-cm-thick concrete shield wall and enter the Target Bay.

Each beam has a unique identification: the 15 beams propagating west are referred to as "legs." The 60 beams that emerge from the stage-D splitter are called "beams." Figure 2.5 shows the OMEGA beam-numbering convention.



G5626J1

Figure 2.5  
OMEGA beam designations as viewed from the Target Bay.

In the Target Bay, each beam encounters a stage-F alignment sensor package (F-ASP), which provides the alignment reference for the laser beamlines. The F-ASP's are housed in six structures constructed of a cast epoxy/granite composite. These massive structures (20,000 kg each) ensure the thermal and vibrational stability necessary for the required  $\sim 5\text{-}\mu\text{rad}$  system-alignment accuracy. Also in these structures are optical pickoffs that distribute a fraction of the beam energy to the alignment, energy, and pulse-shape diagnostics.

The F-ASP's provide the reference to which IR and UV beams are aligned. Both IR and UV alignment beams are referenced to the same position on the F-ASP camera. The periscope mirror assembly (PMA) is a moving gantry system that can insert a full-aperture UV beam from the UV alignment table (UVAT) into any of the 60 beamlines aligned to the F-ASP camera.

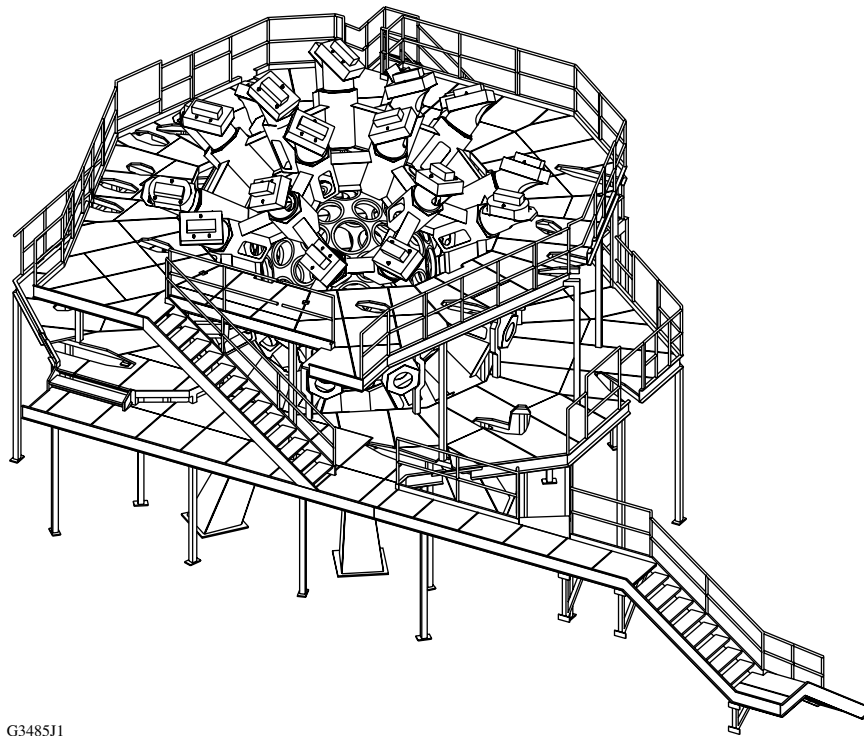
The F-ASP's also provide a sample of each beam via fiber optic to the harmonic energy detector (HED) and to the P510 UV streak-camera system. The HED system consists of integrating spheres that capture and measure a small fraction of the laser-beam energies at the fundamental (1054-nm), second (527-nm), and third (351-nm) harmonics produced by the FCC's. HED diagnostic data is the primary laser-energy diagnostic for OMEGA. The P510 cameras can measure the temporal pulse shape of all ten beams from each cluster. Comparisons between beam-intensity profiles are used to characterize the power balance and infer the time-instantaneous, target-irradiation uniformity.

In the Target Bay, the linear geometry of the laser transitions to the spherical geometry of the target chamber. Each beam is transported to the target chamber via two mirrors: the end mirror on the beam axis and the target mirror on the target mirror structure (TMS). The focus lens assembly (FLAS), which holds the focus lens and the DPP for each beam, is mounted on the chamber. The focused beam enters the evacuated target chamber through a flat blast window assembly (BWA), which has two optics: a vacuum window and a thin debris shield. The TMS supports the target mirrors, the target chamber, and its ancillary systems and is surrounded by the TMS platform for personnel access. These are shown in Fig. 2.6.

#### **2.2.4 Laser-Drivers Subsystem**

The laser-drivers subsystem consists of the equipment that provides the temporally shaped seed pulses to the beamlines subsystem, and a "fiducial" pulse train that provides a timing reference for many of the laser and target diagnostics. The electronic timing system, called the Hardware Timing System (HTS), is used to trigger time-critical functions throughout the OMEGA system and is synchronized to the laser by an rf clock located within the laser-drivers subsystem.

The two separate seed-pulse drivers are called the SSD and the backlighter. The subsystem is configured so that the SSD driver can be injected into the stage-A splitter, where it would normally continue on to feed each of the three stage-A legs and all 60 beamlines. The backlighter driver can be injected into any one of the stage-A legs, where it can feed 20 beamlines. When this is done, the main or the SSD driver can feed the other two stage-A legs and the remaining 40 beams.



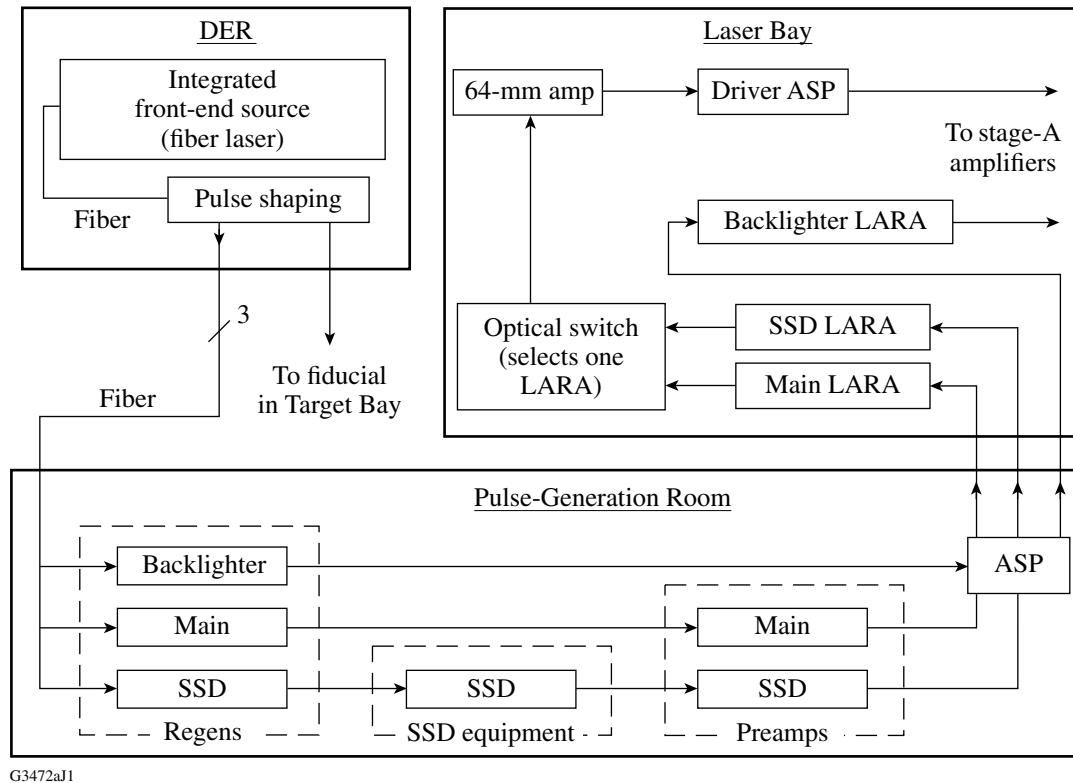
G348511

Figure 2.6  
Target mirror structure and personnel platform.

The names applied to the two driver systems that can seed OMEGA are explained below:

- The “SSD” driver generates a round beam having the appropriate pulse shape and timing needed for shots. It also has the equipment needed to smooth the profile of the beam on target. SSD smoothing is accomplished by more than 100 components including electro-optical modulators and in-house-fabricated holographic diffraction gratings. Because the SSD modulation effect can be readily applied to, or removed from, the pulses provided by this line, the SSD driver has become the primary source for OMEGA.
- The “backlighter” driver equipment is so named because its intended primary use is to seed beams that may be pointed at separate target elements used to produce x rays that backlight the primary target for diagnostic purposes. Because this line does not have an amplifier after its LARA, it is capable of seeding only one 20-beam OMEGA leg. When the backlighter driver is injected into an OMEGA leg, the resulting 20 beams may be directed to all of the same target or diagnostic destinations as beams that are seeded by the SSD driver. This line has no SSD capability.

The laser-driver subsystems, outlined in Fig. 2.7, are located in the DER, the PGR, and the driver line area of the Laser Bay. In addition, a laser-driver system in the Target Bay is used to generate a timing reference (“fiducial”) pulse for diagnostic systems. This fiducial laser is a diode-pumped amplifier, but it produces a comb of pulses. This independent, but synchronous, laser provides IR, green, and deep UV pulses to instruments located throughout the laser facility.



G3472aJ1

Figure 2.7

A block diagram of the laser-driver subsystem. The equipment is located in four areas: Oscillator Room, Pulse-Generation Room, the Laser Bay, and the Target Bay.

The optical pulses used in the OMEGA Laser System originate in the DER, where a master oscillator produces continuous-wave laser light that is temporally shaped for the desired output pulse shape. The DER is adjacent to the PGR and is fiber optically coupled to the PGR. Fiber optics are used throughout the DER for flexibility and alignment insensitivity. The physical separation of the DER and PGR is intended to allow for flexible pulse shaping without impacting the performance or reliability of the PGR subsystems.

The PGR is located below the Laser Bay and is the home of several major elements of the driver line, including pulse selection, regenerative amplification, driver diagnostics, amplification, beam smoothing (the electro-optic frequency modulation and pre-delay components of SSD), and alignment. As shown in Fig. 2.7, the SSD, backlighter, and fiducial regenerative amplifiers are seeded

by pulses from the DER. The regenerative amplifiers (regens) increase the energy of the ~1.0-nJ input pulses to 0.1 mJ, using ~100 round-trips in a laser cavity. Various diagnostics measure the energy, timing, alignment, and stability of the regens.

Beyond the regenerative amplifiers, the pulses in the SSD line encounter the electro-optic modulators and gratings required for SSD. These systems impress the bandwidth and pre-delay required for high irradiation uniformity on target.

To decouple the sensitive PGR optical configuration from heat and electromagnetic interference (EMI) sources, much of the associated electronic equipment is housed in the DER. The various timing circuits, regen cooling system, and majority of the PGR power supplies are located in this room.

The 0.1-mJ outputs from each regen are separately directed upward, via a vertically mounted periscope, to the next set of amplifiers located on the Laser Bay level. These amplifiers are 40-mm, large-aperture ring amplifiers (LARA's). One is provided for each of the SSD and backlighter pulses. Each LARA provides a gain of about 10,000 in four round-trips. The SSD driver is further amplified to 4.5 J by a 64-mm rod amplifier. The pulse is then spatially filtered and propagated to the stage-A beam splitter, where the driver-line pulses are split three ways and injected into the OMEGA power amplifiers.

The backlighter driver generates a 1.5-J laser pulse capable of driving one of the three legs from the A-split in lieu of the SSD driver pulses. The backlighter pulse arrives at the stage-A splitter by a path that is separate from that used by SSD.

### 2.2.5 Amplifier Staging

The power-amplifier section of OMEGA has a 64-mm input aperture and a 20-cm output aperture. The output aperture of the final amplifier was initially determined by the number of beams, the total energy requirement, and damage thresholds for the optical coatings. The amplifier staging comprises four stages of rod amplifiers (A–D) and two stages of disk amplifiers (E and F), all separated by spatial filters. Figure 2.8 provides the details of the final stages. The final aperture of the beam is increased to 28 cm, a factor of 2 in beam area, to reduce the fluence on the UV transport optics.

A total of 93 rod amplifiers are used in stages A–D. The rod amplifier design evolved from the original OMEGA system and incorporates significant mechanical and thermal improvements. Rod amplifiers use de-ionized water cooling for the flashlamps and feature a separate DI/glycol cooling channel along the barrel of the rod. The disk amplifiers for the last two stages are of a conventional box geometry with a 15-cm aperture at stage E followed by a 20-cm aperture at stage F. Each disk amplifier contains four Nd:glass laser disks. The 15-cm stage provides a small-signal gain of 4.2:1, and the 20-cm stage a gain of 3.0:1.

The disk amplifiers, like the rod amplifiers, use water-cooled flash lamps that facilitate operation at a high storage efficiency. The benefits of this are outlined in Chap. 3. Both the 15- and

Stage	C output	D	E	F
Amplifier size		90-mm rod	150-mm disk	200-mm disk
Beam diameter		86 mm	143 mm	191 mm
Nominal energy	25 J		130 J	428 J
				1000 J

G3376bJ2

Figure 2.8

The amplifier staging of the OMEGA laser consists of four stages of rod amplifiers and two stages of disk amplifiers. The early stages compensate for the 1:60 splitting; the last three stages (shown here) provide ~97% of the beamline energy.

20-cm amplifier stages utilize the same power-conditioning and pulse-forming network (PFN). The cooling times for the disk amplifiers permit a 45-min thermal equilibration in support of the nominal 1-h shot cycle. The modular nature of the design allows for the rapid change of flash-lamp pump modules within this shot cycle.

### 2.2.6 Frequency Conversion and UV Transport

Conversion of the 1054-nm IR energy produced by the laser amplifiers into the 351-nm UV energy that is delivered to the target is achieved in the frequency-conversion crystal (FCC) subsystem, located in the Laser Bay at the end of each cluster just before the shield wall. Each of the 60 FCC assemblies has an input polarizer and a cell assembly that includes three crystal optics made from potassium dihydrogen phosphate (KDP) and a UV absorption window. With the correct combination of polarization angle, crystal-axis orientation, and crystal temperature, the first KDP crystal, called the “doubler,” doubles the frequency of part of the incoming 1054-nm beam. The second crystal, called the “tripler,” combines the resulting green photons with the remaining IR photons to efficiently produce UV photons. A second “tripling” crystal provides a capability for efficiently converting up to 1-THz SSD bandwidth. The gimbal mount that holds the crystal assembly has a three-axis motorized positioner and several parameters manually set with the initial crystal configuration. The temperature of each FCC is kept stable by an insulated enclosure and is sensed to allow for the gimbal axes to be angularly tuned in response to minor changes in temperature. The temperature tuning is achieved through the computer control system to maximize the frequency-conversion efficiency.

After the IR beam is converted to the UV, it passes through the shield wall and through the Stage-F alignment sensor package (F-ASP). The UV transport system utilizes two UV high-reflector (HR) mirrors per beam to direct the UV beam exiting the F-ASP to the target chamber.

The unconverted light, residual IR and green, are transmitted through the UV HR's and terminated on beam dumps. Very little unconverted light is delivered to the targets. The UV beams are focused onto the target using 1.8-m-focal-length,  $f/6.7$ , fused-silica aspheric lenses. These lenses are mounted in precision mounts to accurately control the lens position for focusing. This subsystem is called the focus lens adjustment system, or FLAS. A distributed phase plate (DPP) can be mounted on the input end of the FLAS. The DPP optics create a uniform, repeatable spot approximately the size of a typical fusion capsule. Because some experiment campaigns do not irradiate spherical capsules, these optics are removable. Different DPP designs are available to create different irradiation conditions, such as elliptical indirect-direct irradiation (IDI) for optimized coupling to a hohlraum, or polar-direct-drive (PDD) DPP's for simulating polar-drive conditions on the NIF.

The F-ASP's and periscope mirror assembly (PMA) are located along the shield wall, and the north and south ends of the Target Bay are filled with the end-mirror structures (EMS's). A personnel platform surrounds the target mirror structure (TMS) and provides three working levels, enabling one to access all the ports on the target chamber, as well as the transport optics. The north EMS platform supports the fiducial laser, and a laser-diagnostic station has been deployed on the south EMS platform.

The TMS is central to the target area, which supports the target mirrors and target chamber. The 3.3-m-diam chamber is where targets are irradiated and the various diagnostics are supported. The diagnostic suite has both fixed and flexible diagnostic platforms. Fixed diagnostics include x-ray pinhole cameras that capture time-integrated images of the target emission, Kirkpatrick–Baez (KB) microscopes, and x-ray and neutron streak cameras that record time-resolved target events. There are also neutron time-of-flight (nTOF) instruments and other fixed diagnostics.

Flexible accommodations for experimental diagnostics are provided by ten-inch manipulators (TIM's). Six of these subsystems are installed on the target chamber. Each provides mechanical, vacuum, and electrical/control support and positioning for any compatible instrument that must be positioned near the center of the target chamber. TIM diagnostics can be exchanged between shots, typically within a shot cycle. Heavy TIM loads; for example, six time-resolved instruments running film can impact the cycle time. Additionally, diagnostic changes in the TIM's can have an impact. If there are any questions, LLE personnel can be contacted and can assist any PI interested in making prudent decisions regarding cycle optimization. Also installed on the chamber are the Target Viewing Systems (TVS's), the system used to position ambient-temperature targets, the upper and lower pylon elements of the Cryogenic Target Handling System (CTHS), and the cryogenic pumps used to create the high-vacuum environment.

### 2.2.7 Optical Alignment

Because the high-energy pulsed beam is converted from IR to UV, the OMEGA alignment system must include both IR and UV sources. A hand-off between the two alignment sources takes place at the 60 F-ASP's. These utilize achromatic optics so that they can function at both wavelengths and are located in the Target Bay just before the end mirrors. Each F-ASP includes a special full-aperture pickoff optic that reflects 4% of the beam energy into the diagnostic subsystem, while making

it possible for the remainder to propagate onward to the end mirror. During the alignment process, a 4% sample of the alignment beam being used is directed to the alignment sensor. On shot, the 4% sample of the high-energy pulse is directed to beam-performance diagnostics, the harmonic energy detector (diagnostic) (HED), the P510 60-beam streak-camera system, and the UV spectrometer.

The IR portion of the OMEGA system is aligned using a 1054-nm Nd-doped yttrium lithium fluoride (Nd:YLF) laser that is located on the infrared alignment table (IRAT) and is injected into the system at the A-splitter. The beam train is aligned in a progression toward the target using a sensor package: the A-splitter, 15 sensor packages at stage C, and ending at pointing references in each of the 60 F-ASP's.

The UV portion of the system is aligned using a 351-nm cw laser mounted on the UV alignment table (UVAT) on the centerline of the system near the west wall of the Target Bay. The UVAT optics project separate full-aperture alignment beams northward and southward from the table into corresponding periscope mirror assemblies (PMA's). Each PMA functions to position movable mirrors at specific locations on the shield wall. These mirrors inject the alignment beam into one beamline at a time on each side of the bay.

Co-aligning the IR and UV alignment beams in each beamline is achieved by steering the PMA mirrors to point the UV alignment beam to the pointing reference in the F-ASP. The portion of the UV alignment beam that passes through the pickoff optic is then steered to the target by moving the transport mirrors. To guide this process the UV reflections from a surrogate target are transmitted back to an alignment sensor package on the UVAT. The north/south symmetry makes it possible to simultaneously align one north side beam and one south side beam.

### 2.2.8 Laser Diagnostics

Beam-energy measurements are required at various points in the laser chain. The most important measurement is made just after the FCC's, where a second-order Fresnel reflection from two uncoated optical surfaces transports 0.16% of the beam energy into a harmonic energy diagnostic (HED) package. The first uncoated surface is the primary pickoff that passes 96% of the energy to the target. The second is on a flip-in optic that directs 0.16% of energy to an integrating sphere via an evacuated optical relay. The optical layout ensures that the beam image plane is relayed to the rear surface of an integrating sphere. A fiber-optic pickup in each sphere transfers the light to a spectrometer coupled to a scientific CCD camera. There is one spectrometer/CCD unit for the 30 beams on each of the north and south sides of the Target Bay. The HED spectrometers are calibrated using 60 full-aperture calorimeters that can be inserted into the beam to measure its total energy. These calorimeters are of a conventional absorber/thermopile design.

The UV delivered to target is equal to the energy measured by the HED and multiplied by the passive transmission of the UV transport optics. Each beam has two UV high-reflector mirrors, a distributed phase plate, a focus lens, a vacuum window, and a debris shield. An instrument called the OMEGA Transport Instrumentation System (OTIS) measures the cumulative transmission of the ten optical surfaces and four substrates. OTIS consists of a CCD-based ratiometer embedded in

the UVAT and a special reflective sphere inserted into the target chamber. This system is capable of characterizing the UV transport with better than 1% precision.

An instrument called the P510 streak camera measures temporal pulse shapes of the output of each of the 60 beams. The instrument system consists of six separate instruments, each of which measures the ten beams from a cluster. These cameras have very high temporal bandwidth for a high-fidelity time history of the irradiation on target. Because the UV shape on target is one of the critical parameters in which an investigator conducting experiments on OMEGA is interested, this system is calibrated frequently for optimal performance.

### 2.2.9 Control System

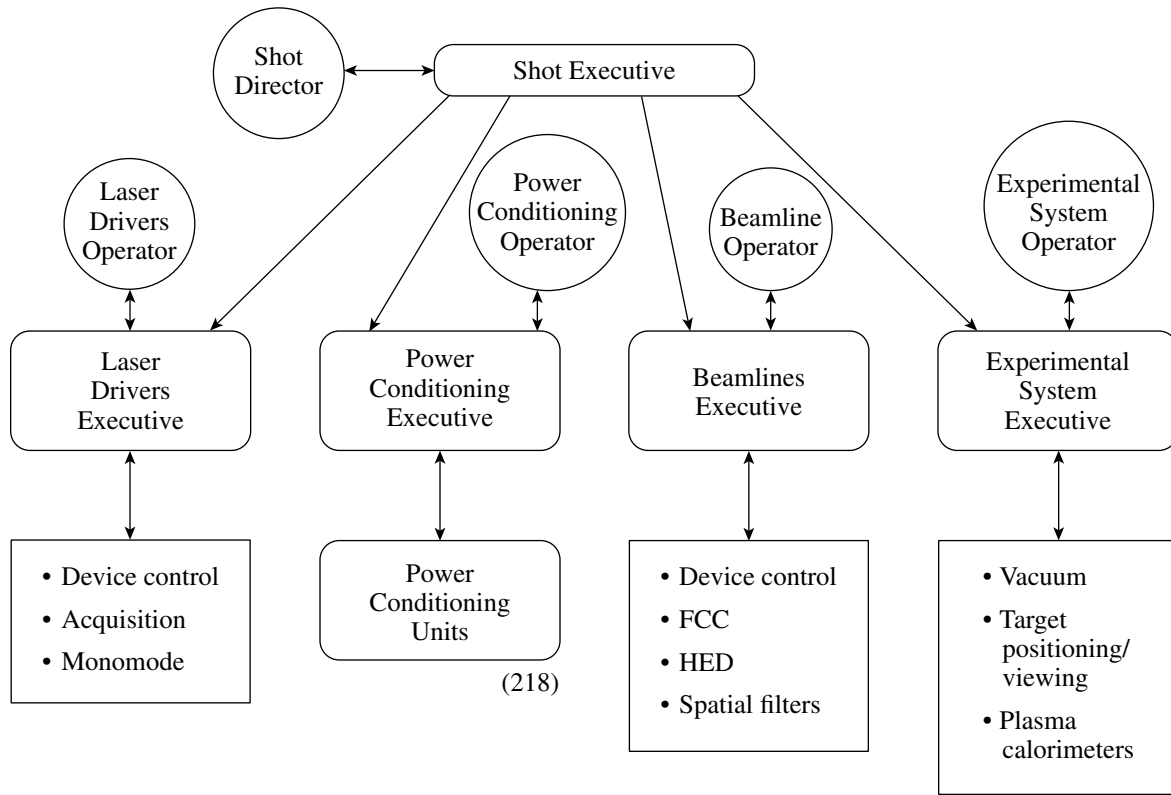
The OMEGA control system provides the system operators with remote control of subsystems, displays of sensor data, and safe sequencing of key processes. The control system also collects and records information about each shot. Operator interfaces are provided in the Control Room and throughout the facility.

#### (a) *Functional Subsystems*

The control-system architecture reflects the hierarchical subsystem configuration of OMEGA. Four autonomous consoles in the Control Room enable the respective trained operators to operate each subsystem. During shot operations, the subsystem functions are coordinated by a Shot Director who uses a fifth, supervisory, control station. Figure 2.9 illustrates this arrangement.

Communication between the operators and the supporting technicians is facilitated by a headset-based intercom and a facility public address system. This verbal communication is supplemented by messages that pass between the application programs running on the computers. High-level application-to-application communication uses a standardized OMEGA intercommunication protocol (OIP) that conveys limited system status and control information in both directions. Figure 2.10 shows two examples of the “generic executive” graphical user interface (GUI) that portrays the status information to the operators. Specific versions of the generic executive are configured as the Shot Executive (SE), Laser Drivers Executive (LDE), Beamlines Executive (BE), and Experimental Executive (EE). [Although the Power Conditioning Executive (PCE) is functionally similar, it is not based on the same generic code as the other executives. Yet another variation is the Facility Interlock Executive (FIE), which is used primarily by the Shot Director, to manage room access and warnings.]

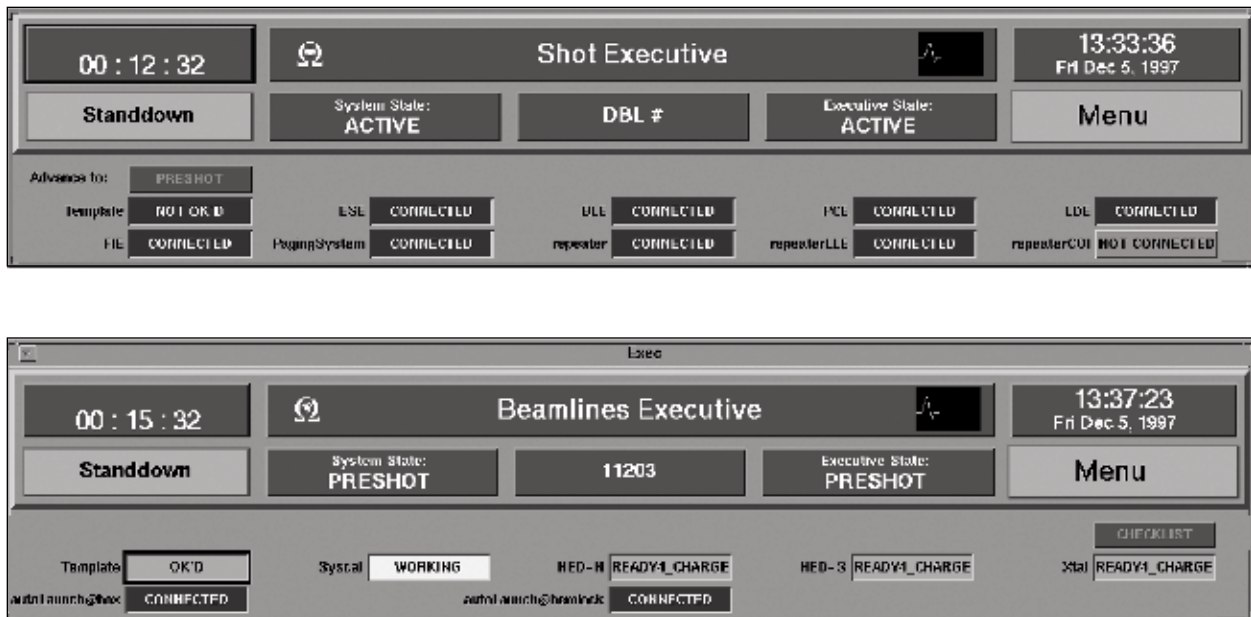
Each executive provides a top-level operator interface for the subsystem and controls and receives information from devices in the bays by communicating with one or more “intermediate” processors over bus extensions, the Ethernet, or other standard communication links. These intermediate computers serve to relieve the executive of routine computation and downward communication tasks. Each of the subsystem executives monitors the applications required for configuring and executing a shot at that console. All executive processors are synchronized to the shot sequence by the Shot Executive.



G4518cJ1

Figure 2.9

The top-level architecture of the OMEGA Control System. (Circles represent human operators; boxes represent applications running on computer workstations.) Three levels of computers are used to provide a system with appropriately distributed processing capabilities. Operators use executive and subsystem-specific applications to operate numerous microprocessor-controlled devices via local networks. The Shot Director monitors and coordinates the subsystem activities.



G4582J1

Figure 2.10

Each Control Room operator is provided with a standardized display of the status of the overall OMEGA system and of the sub-tier processes critical to his or her functions. Two examples are shown here.

(b) *Control Room and Control Stations*

The OMEGA Control Room, located on the second floor of LLE, is the focus of operations. Figure 2.11 depicts a layout of the Control Room, showing the space allocations for control, operations, and planning and data analysis activities. The equipment is arranged to enable the operators to work together and to minimize distractions.

(c) *Shots and System States*

The control system facilitates the operational activities that maintain the system, prepare it for a shot, execute the shot, and record the shot results. Computer network communication is used to coordinate actions requiring synchronization to within  $\sim 1$  s. The precision timing required to execute and diagnose a shot is provided by the hardware timing system (HTS). A “handoff” between the two levels of timing control takes place 20 s before a shot is triggered.

The approach to system operations makes use of the concept of a “shot cycle,” consisting of a sequence of “system states” and a number of distinct “shot types.” The system states partition the activities into known situations for communications and coordination. The shot types identify the extent to which the high-energy pulsed beam is propagated and the degree of system-wide coordination that is required.

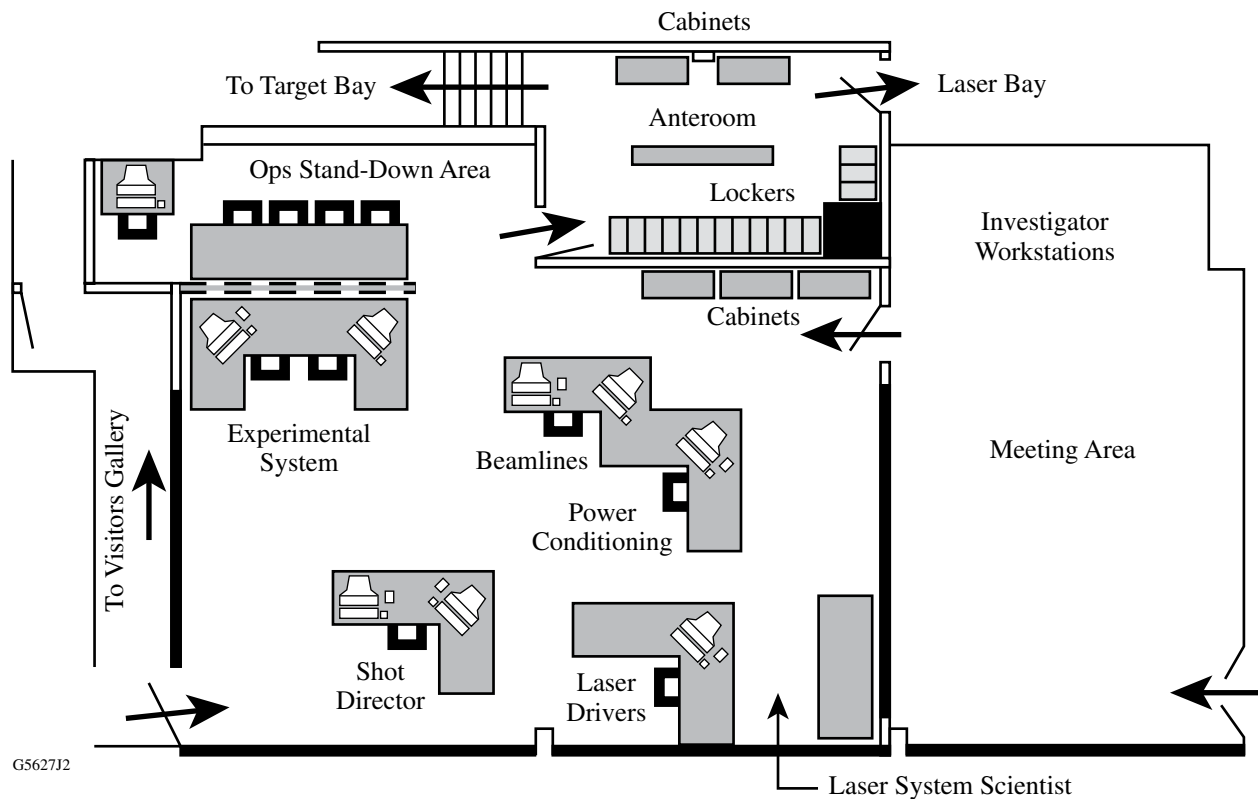


Figure 2.11

The Control Room workstations are arranged to allow the operators to work together with minimal distraction. A separate conference room is used for briefings, data assessment, and planning. The Target and Laser Bays are accessed through the Control Room.

Figure 2.12 illustrates the system-state sequence that is executed for every type of shot. In the “active” state, the system is not formally preparing for a specific shot and the subsystems are operated independently for maintenance or setup. Formal preparations for a shot are initiated by the Shot Director (SD) who uses the Shot Executive (SE) to specify a shot type and other key parameters and to communicate them to the other operators via the subsystem executives. The act of transmitting this “master template” information marks the transition of the system from the active state to the “pre-shot” state. The SE also transmits a “shot number,” which is the index to be used when the data from the intended shot is logged. Each subsystem operator reviews the setup information, signals approval to the SD, and proceeds to prepare for the shot.

When a subsystem has been readied, the operator signals the SD using a “checklist” button on the executive GUI. The SD then reviews key details of the setup with the operator before signifying concurrence on the Shot Executive. In the special case of the power conditioning subsystem, this process consists of the SD reviewing and approving the power conditioning “template,” which details the online/offline status of the power conditioning units (PCU’s) and the voltage commands that will be sent to them for the shot. When this critical safety check is complete, the SD authorizes the transmission (“download”) of the template values.

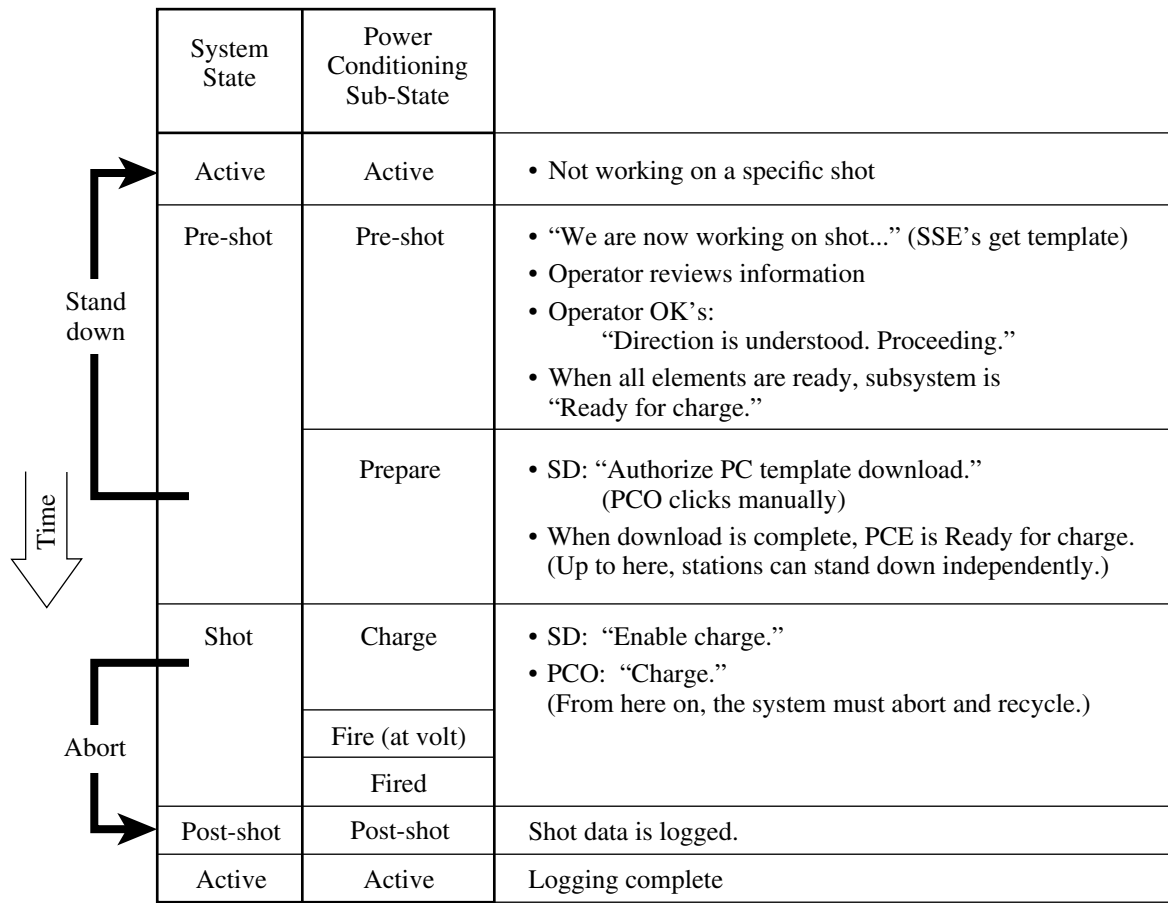


Figure 2.12  
 The OMEGA shot cycle is a sequence of system states. In the “active” state, the system is not formally preparing for a specific shot and the subsystems are operated independently for maintenance or setup. The pre-shot/shot/post-shot sequence is repeated for each shot attempt. The power conditioning subsystem has sub-states.

When all necessary subsystems are ready for the shot, the SD authorizes the power conditioning operator to charge the PCU’s. This marks the transition from the pre-shot state to the “shot” system state. Within the shot system state, the power conditioning subsystem has sub-states that are not reflected in the other processes. These track the major steps of the power conditioning subsystem sequence. Once the charge command has been issued, the power conditioning subsystem controls the laser system to within 10 s of the shot and then enables the key system elements to proceed on the basis of electrical master timing signals from the HTS.

The events synchronized by network messages include activating high-voltage diagnostic power supplies, acquiring background data, and “arming” elements so that they will respond to hardware triggers. The events synchronized by the hardware timing signals include selecting the optical pulses in the laser-drivers subsystem, triggering the electrical discharges that drive the flash lamps in the laser amplifiers, and operating diagnostic instruments.

Once the software and hardware sequencing has proceeded through the issuing of the shot triggers, the system enters the “post-shot” state and each of the system elements that has acquired shot-related data proceeds to log that data to the system database. As the logging is completed, each element effectively reverts to its “active” state. When all of the elements have completed this process, the system is formally in the active state and ready to initiate another shot cycle.

(d) *Stand-Down and Abort*

The shot cycle can be interrupted by either a “stand-down” or an “abort.” If a problem arises or a change of plans occurs prior to the system entering the “shot state” (the PCU’s have not started to charge), the system can “stand down” to the active state. When the situation is cleared up, a new shot cycle can be initiated. Each subsystem can also stand down independently. In this case, the *system* remains in the pre-shot state, and the subsystem will automatically advance into its pre-shot state as soon as it is ready to do so. Because a stand-down does not cause shot data to be logged, the “shot number” is not incremented.

If a critical problem arises after charging has started, the shot is normally stopped by the abort process: Each of the executive GUI’s has an ABORT button that can be used to initiate the process by signaling the PCE to execute an “abort.” All of the other software elements are also notified so that they can respond as needed. When an abort is signaled, the PCE immediately prevents the HTS from issuing the critical triggers and issues commands that dump the energy in the capacitors located in the PCU’s. Power conditioning and other subsystems then log data and the system proceeds to the active state. In this case, the “shot number” is used and the next shot attempt will be associated with the next sequential number.

The Shot Director can also stop a shot by pressing a switch that is hard-wired to the electric power substation that powers the PCU’s, shutting off all its output. This, in turn, dumps the energy in the capacitors and renders the system safe, even if a software or communication failure has occurred.

While the software-based abort and the hard-wired dump are effective in stopping a shot up to within about 1 s before the shot trigger, some conditions that necessitate preventing a shot can be detected only in the area of 10 to 100 ms before the shot trigger. These include the target moving or not being in the correct location near the center of the target chamber or an error in removing the shroud from a cryogenic target. A mechanism that spoils the seed pulse in the laser-drivers subsystem is used to address these conditions. This “driver abort” is automatically initiated by computer logic associated with a target-detection subsystem. The action interrupts the trigger for the regenerative amplifier in the driver. The pulse that then propagates to the power amplifiers is too low in energy to be amplified to normal levels in the remainder of the system. This prevents laser damage caused by energy passing through the target chamber.

(e) *Shot Types*

Not all shots on OMEGA are target shots used for physics research. Many are used for system preparation, checkout and evaluation, or laser-technology research and development. This has made it necessary to consider categories, or types, of shots. The seven “shot types” that have been defined are

Type	Description
1	Driver only
2	Non-propagating (no driver)
3	Propagating to the Stage-A splitter
4	Propagating to the Stage-D splitter
5	Propagating to the Stage-F alignment sensor package
6	Target shot with low (or no) neutron yield
7	Target shot with high neutron yield

The shot type establishes which of the executive processes must be involved in the shot, the location at which propagation stops, and which bays must be closed to access.

In addition, each of the seven shots may be simulated as a “trigger test” shot: the system-state sequence is executed as it would be for an actual shot and the HTS triggers are produced, but no PCU’s are charged and the seed pulse is not amplified beyond the driver regenerative amplifiers. The two variations are

- Null Template Trigger Test: No PCU’s are included in the Power Conditioning Template.
- Zero Volts Trigger Test: One or more PCU’s are included, but the charge voltages are set to zero.

It is also possible to produce the HTS triggers without executing the system-state sequence. This is called a “Timing Test.”

(f) *Shot Request Forms*

Executing effective and safe experimental shots requires a complete and detailed specification of the facility configuration and laser-operating parameters, extensive advance planning, and many hours of system preparation prior to and during the actual shot day. The Shot Request Form (SRF) is the primary vehicle for recording and communicating the specifications for a shot. A separate SRF is used for each target shot. Supplemental tools and forms are also generally used in planning and communicating the sequences of related shots that are referred to as “campaigns.”

The SRF is a database object that is created within the LLE computer system primarily via inputs made at a web-based SRF user interface. This interface consists of a series of pages or screens called “forms” that collect information of various types. The forms include

- General – PI's, campaign identification, planned date, planned order, ...
- Driver – pulse shape, SSD modulation, ...
- Target – characteristics, unique identifier, ...
- Beams – groups defined by energy, pointing, focus, ...

Target diagnostics are specified via a hierarchical series of groupings and setup forms.

Each SRF is automatically assigned a unique, sequential, identifying number at the time it is created. Appropriate controls are applied to limit both read and write access to the records. Figure 2.13 illustrates some of the relationships between the SRF, the database, and OMEGA operations.

The SRF can be viewed or printed, in part or whole, to provide a standard format for review and implementation. On shot day, SRF data values are also accessed directly by the OMEGA Control System and used to assist the operators in preparing for and executing the shot. Once an SRF has been used to specify a system shot, it is considered expended and will not be reused. The SRF data values are retained indefinitely. The SRF values, indexed by the unique identifying number, may be retrieved for use in data assessment and can be copied to create new SRF's.

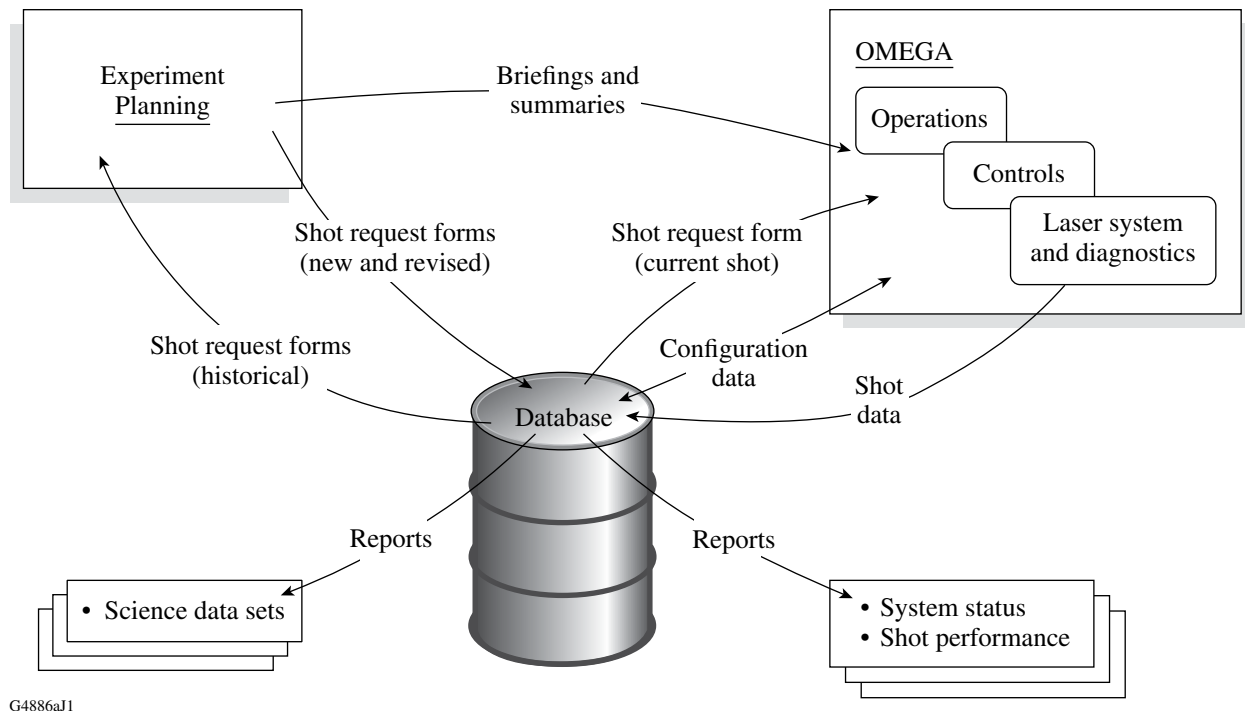


Figure 2.13

The OMEGA database plays a significant role in the planning, execution, and evaluation of shots. The detailed plans for experimental campaigns are embodied in Shot Request Forms (SRF's), which are stored in the database. SRF data is used to configure the OMEGA system for the shot. On-the-shot data acquired by the system and the laser and target diagnostics is recorded in the database.

(g) *Data Acquisition and Archiving*

Both system-configuration and diagnostic-sensor data are logged for each shot. The system-configuration data consists of all the parameters that are sensed by the computer system and all the parameters that can be altered by inputs to the software. Diagnostic data is generally stored locally during a shot and transferred to the archive within minutes after the shot.

(h) *Data Reduction*

A standard set of data reduction routines is used in support of system operations to make it possible for assessments to be made immediately after the shot. Detailed reduction of most target-diagnostic data is performed by the investigators well after the shot.

## 2.3 OMEGA FEATURES AND RECENT ENHANCEMENTS

Improvements to the OMEGA Laser System have continued to maintain it as a unique resource for performing a wide variety of precision experiments. Direct-drive-implosion experiments have benefited from improvements to the power balance (Sec. 2.3.1), advances in pulse-shaping technology (Sec. 2.3.2), and implementation of a new set of phase plates (Sec. 2.3.3). Section 2.3.3 also describes a set of elliptical phase plates that have enhanced the quality of indirect-drive experiments carried out under the National Ignition Campaign (NIC). Plasma-physics experiments have benefited from the addition of optics enabling one OMEGA beam to be diverted and focused on target as either a second-harmonic beam for laser-plasma interaction experiments or a fourth-harmonic beam for Thomson scattering (Sec. 2.3.4).

OMEGA laser-performance diagnostics have been enhanced by adding a novel UV spectrometer with a separate channel for each OMEGA beam (Sec. 2.3.5). The spectrometer monitors the performance of the high-bandwidth SSD system on OMEGA, detects misalignment of frequency-conversion crystals, and diagnoses self-phase modulation within the laser system.

A new Target Chamber Tritium Recovery System (TC-TRS) has been installed to support high-activity cryogenic DT targets (Sec. 2.3.6). Improvements have been made to OMEGA Operations software to accommodate both new OMEGA capabilities and requirements related to OMEGA EP (Sec. 2.3.7). A significant effort continues to be directed to supporting external users, who account for more than 60% of OMEGA shots (Sec. 2.3.8). Operational statistics (Sec. 2.3.9) show that high levels of system reliability and experimental effectiveness have been maintained.

### 2.3.1 Power Balance

OMEGA was designed to achieve very low beam-to-beam variations in both power and energy on target. Very tight tolerances were placed on a number of important subsystems, including energy measurement and power conditioning. The performance of these subsystems meets or exceeds the specifications. As a result, the system meets its power-balance specification of 5% rms beam-to-beam.

Energy balance is necessary to ensure power balance, but it is not sufficient. Because of the intrinsically nonlinear nature of the laser system, two beamlines can generate the same energy with different output pulse shapes, even though all beamlines are fed with the same input pulse shape derived from the single master oscillator. To obtain good power balance, it is necessary to match the gains and losses of all beamlines at each stage, and to control the optical splitters with which the driver beam is successively divided into 60 individual beams. The gains are measured by firing a single stage of the system and recording the signal using a special pickoff in the final (stage-F) spatial filter that feeds an additional set of fibers attached to the harmonic energy diagnostic (HED) system.<sup>1</sup> This signal, divided by the signal from a reference shot taken without firing the stage being measured, provides the relative small-signal gain of the stage. Major differences in gain generally represent faults in the amplifiers that are corrected. Minor differences in gain are corrected by making adjustments to the charge voltage for the amplifier. Using this procedure, the small-signal gains of the amplifiers can be matched to better than 1%.

While the inter-stage losses are difficult to measure directly, the specifications on the optics and their maintenance ensure that losses between stages are matched to better than the required 2% per stage.

Once the amplifier gains are matched, the split ratios are adjusted to balance the output energies. Because of unavoidable differences among the beamlines, it is not optimum to exactly balance the input energies. Matching the splits is determined by firing subsets of the system and measuring the output energies. Using this data as input, the splits are then set using an automated adjustment system.

A test shot with only stages A–D fired is used to evaluate the quality of the split adjustment. Residual errors are compensated by adjusting the gains of the D amplifiers. Based on a full-system shot, the gains of the F amplifiers are then adjusted to match the IR energies input to the frequency-conversion crystals. This technique is a variation of that described in Ref. 1. IR energy balance into the frequency-conversion crystals is typically at the 0.6% level after this procedure, with the UV out of the crystals matched to 2.2%. The on-target energy balance that results is typically at the 3.5% level or better, this higher number reflecting variations among beamlines in the transport optics from the crystals to the target.

Simulations of the system, combined with selected measurements from the P510 streak cameras and system-energy measurements, indicate that, after power balancing, the required 5% beam-to-beam power matching at the output of the frequency-conversion crystals is almost certainly being obtained, even for strongly shaped pulses. At present this level of power balance cannot be fully confirmed with streak-camera measurements since not all 60 channels of the P510 system have the required precision.

Refinements to the data-reduction software are needed to obtain the required time-base accuracy and handle bandwidth mismatches (different cameras generate different amounts of spreading of the sharp rising and falling edges of the pulses). The single-master-oscillator configuration of the

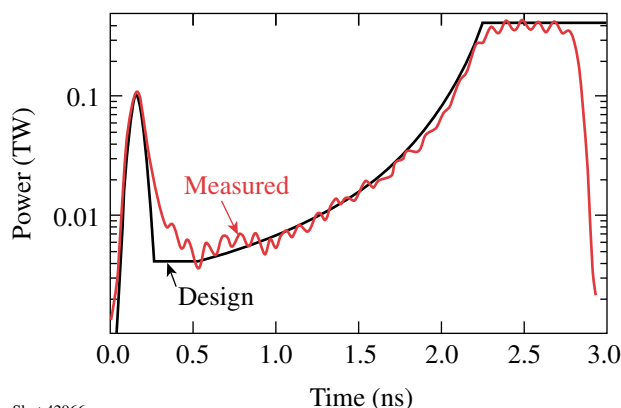
OMEGA laser makes it possible for certain kinds of measured imbalance to be readily identified as arising from instrumental error. Time-base variations and bandwidth mismatch among the channels are readily apparent. By eliminating those channels that clearly suffer from these defects, it is possible to use a subset of the measurements to confirm the model's predictions of power balance.

There are several optics between the energy- and power-measurement pickoffs and the target. To obtain the UV energy and power balance on target, the losses caused by these optics must be measured. This is done by propagating the UV-alignment laser beam through these optics to the target chamber and back and using the very consistent Fresnel reflection from a glass sphere placed at target chamber center. This allows for absolute transport measurements to be made with an accuracy of better than 1%. Based on these measurements, transport optics are replaced in such a way as to maximize the uniformity of the net beam-to-beam transport. Transport matching to about 1% is generally obtained.

The power-balance strategy outlined above tends to provide the best balance at the time in the pulse when two thirds of the energy has been delivered. This is typically at the peak power level for shaped pulses. It is generally considered preferable to have the best power balance occur in the foot of the pulse. When the P510 data reduction is improved to the point that sufficiently good power measurements can be made in the foot, this data will be used to adjust the gain of the F amplifiers to optimize balance in the foot of the pulse. This can be accomplished with very little degradation of the power balance later in the pulse.

### 2.3.2 Precision Pulse Shaping

Several advances have been made in precision pulse shaping on the OMEGA Laser System. An integrated front-end source has provided shaped pulses with higher reliability than previous systems. Figure 2.14 shows the design template and the measured ultraviolet laser pulse produced on target for a low-adiabat pulse shape. This includes a narrow picket pulse (~80 ps) on top of a low-intensity foot followed by a high-intensity drive pulse. Such pulses are required for ignition-scaled cryogenic target experiments. The agreement between the designed and measured shapes is excellent, particularly for the picket energy, the 100:1 contrast between the foot and drive pulses, and the rising edge of the drive pulse.



Shot 42966  
U557JX

Figure 2.14  
Designed and measured single-beam pulse shapes for a low-adiabat cryogenic target implosion on OMEGA (shot 42966).

The capability to routinely produce a picket with stable width and amplitude combined with a shaped pulse is now standard on OMEGA. A method for generating stable double pickets has also been developed and has been used in target experiments on OMEGA.

### 2.3.3 Phase Plates

A major requirement for successful laser fusion is the uniform irradiation of fuel capsules. For high-power, solid-state laser drivers, the major source of irradiation nonuniformity is the intensity distribution of the individual frequency-tripled beams at the target plane. The beams' irradiation nonuniformities are caused primarily by spatial variations in the near-field phase front that accumulate as the pulse propagates through the air, the amplifiers, and the transport optics. Phase plates at the end of a laser beam<sup>2-4</sup> modify the beam's spatial coherence, changing its focusing properties and shifting the on-target energy toward the higher spatial frequencies that can be smoothed using temporal beam-smoothing techniques such as SSD.<sup>5,6</sup> Phase plates limit the effect of shot-to-shot phase errors arising from the amplifiers on the 60-beam on-target irradiation profile. Phase plates also make it possible for the on-target intensity distribution to be shaped according to the needs of different experiments.

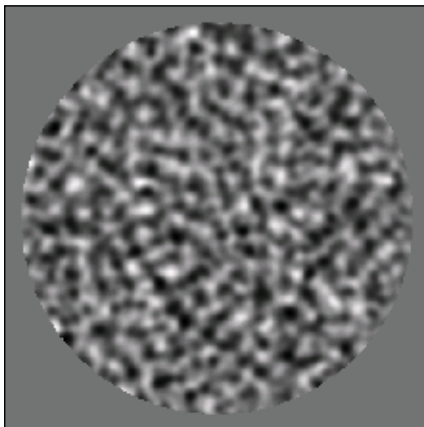
Most experiments carried out on OMEGA require a specific configuration of phase plates. The most prevalently used phase plates, implemented on all 60 OMEGA beams for spherical target-implosion experiments, has an irradiance envelope  $I(r)$  approximated by a rotationally symmetric super-Gaussian profile [ $I(r) \propto \exp(-r/r_0)^n$ , where  $r$  is radius,  $r_0 = 380 \mu\text{m}$ , and  $n \approx 7$ ]. When combined with SSD and polarization smoothing, these phase plates (known as "SG4" phase plates since  $n$  is effectively 4 after smoothing) produce the most uniform irradiation conditions available for spherical implosions to date. The latest phase-plate designs, completed in FY13, allow for 40 beams of OMEGA to be directed to a target in an irradiation pattern similar to the direct-drive "polar-drive" configuration on the NIF. This set of phase plates produces circular profiles for the 20 beams that originate near the poles of the target, and elliptical profiles for the 20 beams that are pointed toward the equator. Other experiments conducted on OMEGA rely on a wide variety of available phase plates. These provide alternative spatial profiles for flat-target experiments with 100-, 200-, 300-, and 800- $\mu\text{m}$  spot diameters, some with elliptical profiles for oblique incidence, and some with continuous 1-D patterns of a specific spatial frequency.

Recently produced phase plates are more efficient, uniform, and reproducible than earlier devices because of improvements in lithography, etching, and advances in magnetorheological finishing. A goal of phase-plate design is to generate the desired far-field spatial profile while minimizing wide-angle scattering outside this profile. Improved design techniques, based on simulated annealing and phase-retrieval algorithms, have been developed to improve the shape and profile of the phase-plate focal spot. Greater experience in the design process has resulted in better control of the correlation length in the near-field phase distribution. This makes it possible to select one phase-plate design over another on the basis of overall performance and manufacturability.

For the continuous phase plates currently used,<sup>4</sup> the phase retardation is distributed over the surface by introducing optical-path differences (OPD's) in the form of a continuously varying thickness

$t(x,y)$  of a material with refractive index  $n$ . The OPD is given as  $t(x,y)(n-1)$ . Since the correlation length of the phase plate is much larger than the wavelength of light, the surface relief refracts the light a similar amount for all frequencies, making the on-target spot size relatively independent of wavelength. (This is in contrast to the original phase plates used for fusion applications,<sup>7,8</sup> whose surfaces were made of discrete elements of different thicknesses and suffered from diffraction from the discontinuities.)

Optical lithography is used to generate complex surface-relief structures that are subsequently etched into a glass that is compatible with high-irradiance UV laser light. Mask fabrication, photoresist patterning, and ion-beam etching have been significantly improved at LLE to fabricate 310-mm-diam continuous phase plates for use in OMEGA. Improved photolithographic masks, such as the mask shown in Fig. 2.15, were made using an LVT photographic film writer developed by Eastman Kodak in Rochester, NY. The accurate masks, together with a uniform ultraviolet light source, ensures that the mask transmittance at a point multiplied by the material-removal function of the photoresist is linearly related to the phase difference required by the phase-plate design.



E14636JX

---

Figure 2.15

Surface relief (shown in gray level) on one side of a glass substrate used to form a continuous phase plate.

---

The final fabrication step involves transferring the surface relief into a suitable UV-compatible material. After extensive development of ion-beam etching, transferring photoresist masters into fused-silica glass has become highly reproducible. Fabricating phase plates is performed in class-100 to class-1000 clean-room conditions to limit contamination that can cause losses due to surface-relief scattering, material scattering, and material absorption. An alternative manufacturing process using magnetorheological finishing—a technique originated at LLE—has been developed by outside vendors to fabricate high-quality phase plates for applications requiring small focal spots,<sup>9</sup> for which the gradients of  $t(x,y)$  are small. This process produces very little far-field scatter and defect-free near-field irradiance. It is the baseline process being used to make the NIF indirect-drive phase plates, but its ability to make direct-drive phase plates [which require larger gradients of  $t(x,y)$ ] has still to be determined.

Phase plates are characterized using the OMEGA ultraviolet diagnostic table, which provides a laser-beam characterization capability for up to four beamlines. The table is located on top of the south end-mirror structure, where it has access to beamlines 46, 52, 56, and 57 without conflicting with target chamber access, other diagnostics, or maintenance activities. The on-target irradiation distribution from a single focused laser beam is measured with an equivalent-target-plane charge-coupled device (CCD) camera.<sup>10,11</sup>

Examples of equivalent-target-plane images are given in Fig. 2.16(a) for the “SG4” phase plates recently installed on OMEGA for implosion experiments and the “SG3” phase plates previously used on OMEGA. In both cases 2-D SSD<sup>6</sup> with 1-THz bandwidth<sup>12</sup> and polarization smoothing<sup>13</sup> were used. Lineouts through the images [Fig. 2.16(b)] show that the SG4 phase plates produce significantly flatter profiles than the previous phase plates.

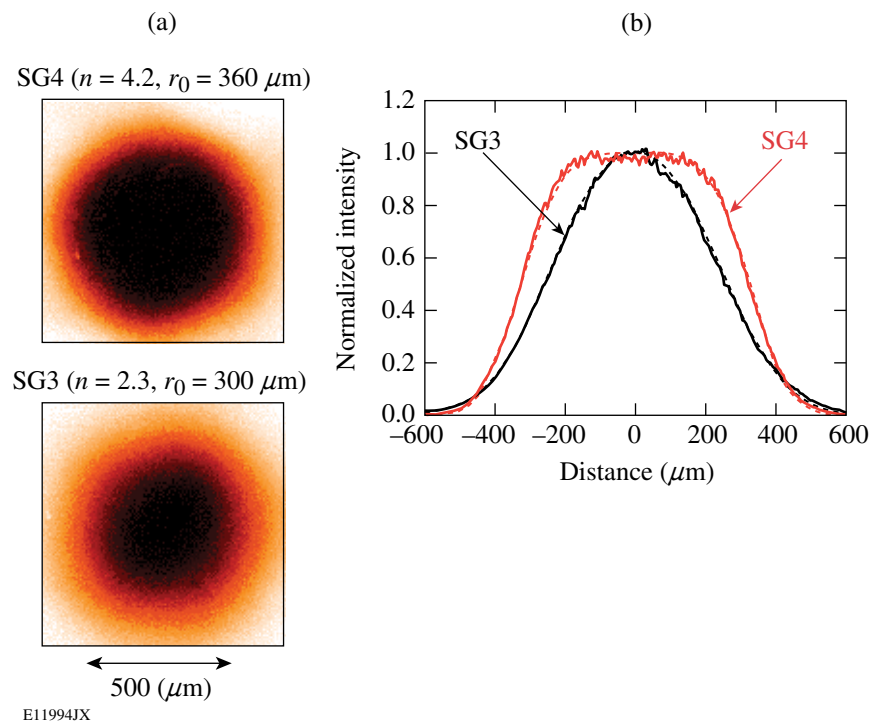


Figure 2.16

(a) Equivalent-target-plane images from the “SG4” phase plates currently used on OMEGA and the “SG3” phase plates previously used on OMEGA. SSD and polarization smoothing are included. (b) Horizontal lineouts through the images of (a), with best fits of the form  $\exp[-(r/r_0)^n]$  shown dashed.

The focal spot from an SG4 phase plate has been characterized outside the focal plane. As seen in Fig. 2.17(a), the azimuthally averaged beam initially becomes less flat as the distance from the best focus increases to 5 mm. As  $z$  increases farther, the profile becomes flatter and then approaches the near-field irradiance profile for very large focal shifts. The measured profiles agree well with ray-tracing simulations.<sup>14</sup> The only significant deviation occurs in a small area near the center of the beam for  $z = 5$  mm, where nonuniformities resulting from phase errors in the near field (not included in the calculation) may not be averaged out effectively; also, speckle in the beam makes it difficult to define a meaningful azimuthal average near the center of the beam. The width of the beam, defined on the basis of the radius encircling 90%, 95%, or 99% of the laser energy, is shown as a function of  $z$  in Fig. 2.17(b).

The profiles shown in Fig. 2.17(a) are for a beam without SSD or polarization smoothing. The  $z = 0$  lineout is a little narrower than the SG4 lineout shown in Fig. 2.16(b) because the angular dispersion associated with SSD (imposed by diffraction gratings early in the laser system) and the far-field displacement between the two polarization components resulting from polarization smoothing cause the beam envelope to be broadened in both directions.

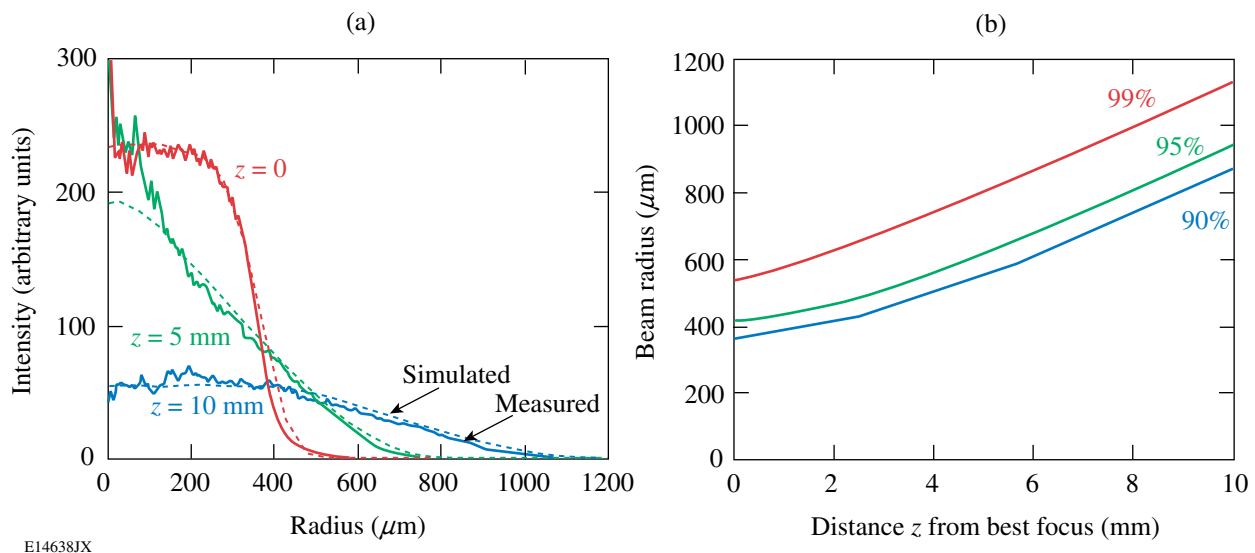


Figure 2.17

(a) Azimuthally averaged radial lineouts of an SG4 phase-plate-intensity distribution (without SSD or polarization smoothing) at three distances  $z$  from best focus. The dashed curves are ray-tracing simulations. (b) Radii of the SG4 beam as a function of  $z$  based on the 90%, 95%, and 99% encircled energy contours.

A set of 40 phase plates has been fabricated for indirect-drive experiments on OMEGA. These phase plates are designed to reach a peak envelope intensity of  $10^{15}$  W/cm<sup>2</sup>. Their shapes are elliptical to provide approximately circular spots when projected onto the laser entrance hole of the hohlraum target. A measured far-field intensity distribution and beam envelope are shown in Fig. 2.18. These phase plates were successfully fabricated using magnetorheological finishing, by Zygo Corporation<sup>15</sup> in collaboration with Lawrence Livermore National Laboratory.

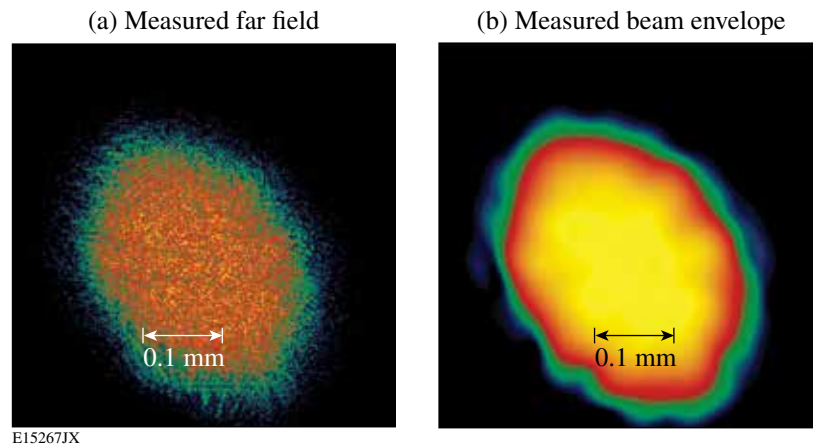


Figure 2.18

(a) Measured far field produced with the elliptical phase plate E-IDI-300 and (b) measured beam envelope. The average intensity  $I_{50}$  is  $1 \times 10^{15}$  W/cm<sup>2</sup>, the peak intensity  $I_{95}$  is  $3.8 \times 10^{15}$  W/cm<sup>2</sup>, the super-Gaussian power  $n$  is 4.1, the  $1/e$  minor diameter is 212  $\mu\text{m}$ , and the  $1/e$  major diameter is 290  $\mu\text{m}$ .

Several other phase plates are available for target experiments on OMEGA. “SG8” phase plates provide  $\sim 800\text{-}\mu\text{m}$ -diam focal spots with a very flat  $\sim 400\text{-}\mu\text{m}$ -diam central portion; they may be approximated as super-Gaussians with  $r_0 = 412 \mu\text{m}$  and  $n = 4.7$ . These phase plates are used for many planar-target experiments including stability, equation-of-state, and long-scale-length-plasma experiments. A set of similar phase plates produces  $800\text{-}\mu\text{m}$ -diam, elliptically shaped spots relative to the beam axis to produce circular spots on target when used at irradiation angles of  $23^\circ$ ,  $48^\circ$ , and  $60^\circ$ . A small number of  $100\text{-}\mu\text{m}$ - and  $200\text{-}\mu\text{m}$ -diam phase plates provide very high irradiance for plasma-physics experiments. Another set of phase plates produces  $300\text{-}\mu\text{m}$ -diam, elliptically shaped spots for use at  $23^\circ$  and  $48^\circ$  irradiation angles. Finally, a novel phase-plate design has produced the one-dimensional pattern in the target plane shown in Fig. 2.19(b) for use in several laser-imprint

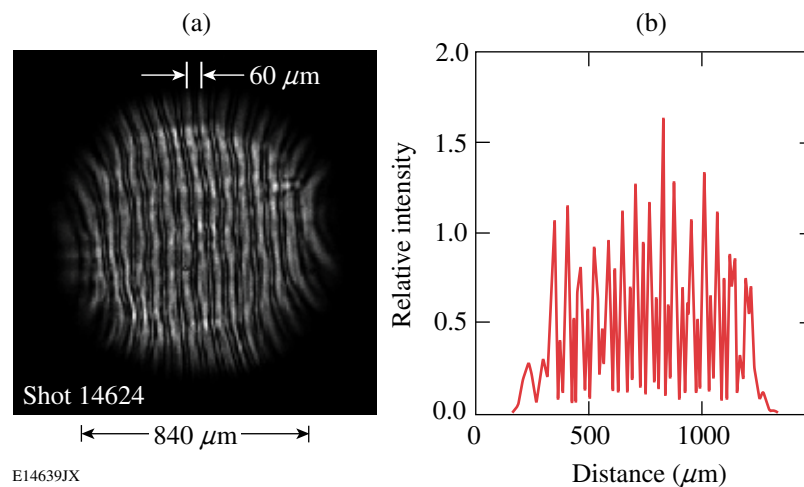


Figure 2.19

(a) Equivalent-target-plane image and (b) one-dimensional lineout of a phase plate designed to provide a  $60\text{-}\mu\text{m}$ -wavelength intensity perturbation.

experiments on OMEGA. Phase plates with intensity perturbations of 30- $\mu\text{m}$  or 60- $\mu\text{m}$  wavelength are available for studying hydrodynamic instabilities.

### 2.3.4 Second-Harmonic and Fourth-Harmonic Capabilities

A second-harmonic ( $2\omega$ ) capability has been implemented on OMEGA. It is available by detuning the triplers in the frequency-conversion cell of one of the OMEGA beams (beam 25) and by using kinematic mirrors, redirecting the beam to port P9 on the target chamber. (A separate port was needed because a new,  $2\omega$  focus lens was required.) Beam pointing, focusing, energy diagnostics, and a dedicated  $2\omega$  phase plate (with a 200- $\mu\text{m}$  spot diameter) are included. The  $2\omega$  beam can be converted to the fourth harmonic ( $4\omega$ ) by inserting a KDP quadrupler into the beam. A half-wave plate can be inserted into the  $4\omega$  beam to rotate its polarization to the desired orientation.

The  $2\omega$  beam is used for  $2\omega$  laser-plasma interaction experiments,<sup>16–18</sup> and the  $4\omega$  beam is used as a probe for Thomson-scattering experiments.<sup>19,20</sup> The  $2\omega$  and  $4\omega$  capabilities were installed as a collaborative effort between LLNL and LLE and were funded through LLNL's laboratory-directed research and development (LDRD) program. A full-aperture backscattering station operating at  $2\omega$  has also been implemented, together with Thomson-scattering diagnostics operating at  $4\omega$ , which measure the absolute, spectrally resolved scattering from the target.

### 2.3.5 UV Spectrometer

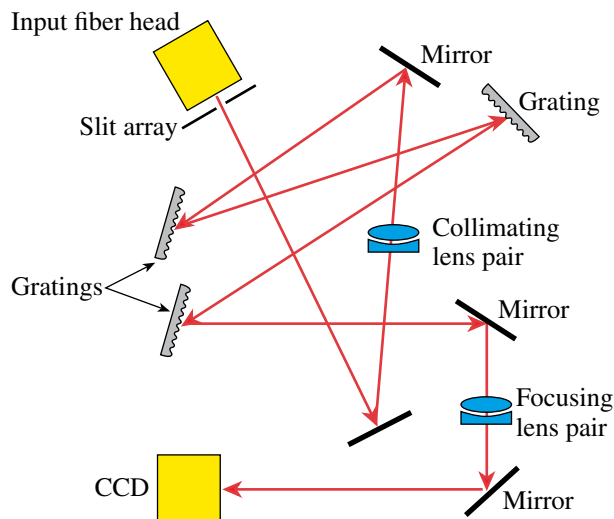
A 63-channel, ultraviolet (UV) spectrometer<sup>21</sup> is now installed on OMEGA. This instrument replaced the previous spectrometer, which was limited to four beams. With an input energy of 1  $\mu\text{J}$  per channel, 63 spectra can be acquired simultaneously on a single multibeam laser shot. The spectrometer has a dispersion at the detector plane of  $8.6 \times 10^{-2}$  picometers (pm)/ $\mu\text{m}$  and a spectral window of 2.4 nm at  $\lambda = 351$  nm. The wavelength resolution varies from 2.5 pm at the center of the field of view, three times better than that of the previous spectrometer, to 6 pm at the edge.

The primary function of the spectrometer is to diagnose the spectral broadening that is imposed on the OMEGA laser beams as part of the implementation of 2-D smoothing by spectral dispersion (SSD).<sup>6,12</sup> To maximize the available bandwidth, limited by the acceptance bandwidth of the potassium-dihydrogen-phosphate (KDP) crystals used for frequency tripling,<sup>22</sup> a second tripler crystal was added to each OMEGA beam, with the two tripler crystals angularly detuned by specified amounts with respect to the direction of propagation.<sup>23,24</sup> To maintain the highest conversion efficiency, the angular detuning of these crystals must be controlled to  $\sim 100$   $\mu\text{rad}$ . Mistuned crystals decrease the UV conversion efficiency and change the spectra of the converted light. While a procedure has been developed to tune the crystals by monitoring the conversion efficiency over a series of nine laser shots, the tuning can drift with time and checks of individual beamlines have revealed that the spectra are different. One objective of the new spectrometer is to determine the tuning state of all the crystals on a single shot and to correct any misaligned crystals, thereby improving the power balance on OMEGA.

A secondary motivation for building the spectrometer was the need to understand and control an intrinsic source of bandwidth on the OMEGA system caused by self-phase modulation (SPM). If the intensity of a laser pulse varies in time, the nonlinear index of refraction produces a time-varying phase.<sup>25</sup> This phase, known as the “*B* integral,” is equal to  $\int n_2 I ds$ , where  $n_2$  is the nonlinear index of refraction,  $I$  is the laser intensity,  $ds$  is an element of the path length, and the integral is over the entire beam path. When this phase varies in time, it produces a frequency shift.

These dual missions determined the specifications of the spectrometer. The spectrometer acquires complete spectra for all OMEGA beams on a single shot. To allow for the possibility of corrupt channels and to incorporate *in-situ* wavelength calibration, the system was constructed with 63 channels. Each channel spans a 0.6-nm bandwidth around  $\lambda = 351$  nm to view the entire SSD-broadened spectrum. With SSD turned off, the spectrometer can resolve spectral features of the order of 3 pm. The light feeding the spectrometer comes from the small fraction of light from each beamline that is split off for diagnostics purposes. To accommodate total UV energies per beamline of 10 to 500 J, the detection system is designed to handle signal levels that vary by a factor of 50, from 20 nJ to 1  $\mu$ J.

A schematic of the spectrometer is shown in Fig. 2.20. Light from a 63-channel fiber bundle passes through a  $3 \times 21$  slit array and a collimating lens pair before reflecting off three mirrors and three gratings. A second lens pair focuses this light onto a CCD. Many spectrometers use reflective optics to image the light through the instrument to avoid chromatic aberrations associated with the refractive elements. However, since this instrument has a limited spectral range, the spectral dispersion in the fused silica can be ignored. The advantage of using refractive optics is that the imaging can be done on axis, allowing a wider field of view than possible with off-axis imaging. The large field of view is required because the spatial extent of the fiber head is  $21 \times 25$  mm<sup>2</sup>.

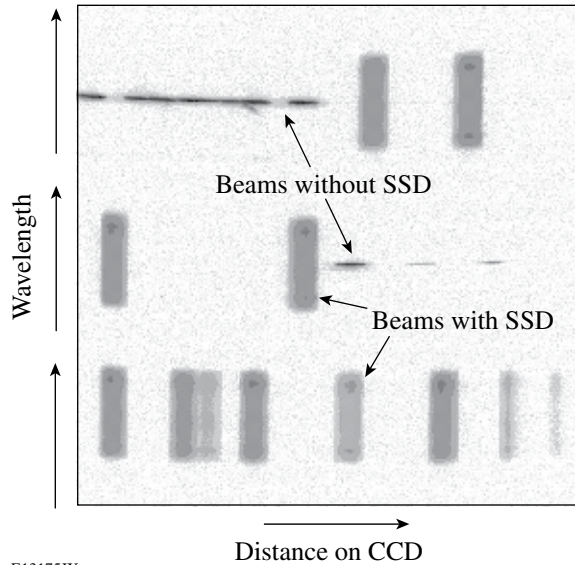


E13178JX

Figure 2.20

Schematic of the 63-channel UV spectrometer. The slit array (one slit per channel) is imaged onto the CCD with spectral dispersion in one direction.

A typical CCD image from the UV spectrometer is shown in Fig. 2.21. The image includes spectra for some beams with SSD and some without. The SSD beams, represented by large rectangular spectra (dispersed in the vertical direction), have approximately the same energy and  $80\times$  the bandwidth of the narrow-line width beams. The 37 missing channels would be interspersed among the 23 channels shown.



E13175JX

---

Figure 2.21

A UV-spectrometer CCD image from shot 37038 showing 23 of the 60 beams, some with and some without SSD. The density is logarithmic.

---

Some representative spectra obtained from images such as those illustrated in Fig. 2.21 are shown in Fig. 2.22. The spectra of Fig. 2.22(a) are from beams with 1-THz SSD and show the characteristic three peaks of the two-tripler frequency-conversion system used on OMEGA.<sup>24</sup> They are produced from a region of the CCD with  $570 \times 100$  pixels by averaging along the 100-pixel spatial direction and show that the spectrum differs from beam to beam. Since the detailed shapes of these spectra depend on the tripler-crystal alignment, the UV spectrometer can potentially aid in crystal tuning.<sup>26</sup>

In Fig. 2.22(b), two spectra taken without SSD are compared. The narrow spectrum, from a low-intensity pulse, is expected to be transform limited and represents the instrument response to a single frequency. The other spectrum, from a high-intensity pulse, illustrates the largest allowed intrinsic spectral broadening on the OMEGA system (resulting mainly from the  $B$  integral). Larger bandwidths can damage the system. The spectrum is asymmetrical because the rising edge of the pulse, which generates the red-shifted wavelengths, is faster than the falling edge, which generates the blue-shifted wavelengths.

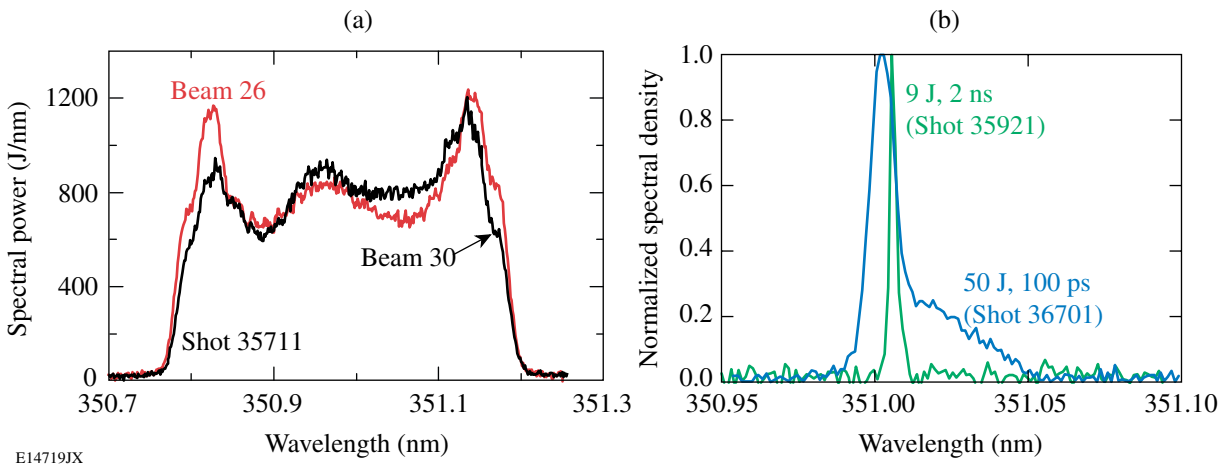


Figure 2.22

(a) Spectra from two beams from a single shot with 1-THz SSD. (b) Spectra from a low-intensity pulse (9 J, 2 ns) and a high-intensity pulse (50 J, 100 ps), both recorded on beam 61, the channel with the highest resolution.

### 2.3.6 Target Chamber Tritium Recovery System

To support high-activity cryogenic DT targets (~0.24 Ci each) while maintaining tritium emissions within environmental release limits (2.2 Ci per year), a Target Chamber Tritium Recovery System (TC-TRS) has been added to the OMEGA target chamber's vacuum-pump exhaust line. This exhaust line also serves the Cryogenic Target Handling System (CTHS) Cart Maintenance Room (CMR) and tritium scrubber.

The TC-TRS uses molecular sieves to collect tritiated water (HTO) from the exhaust effluent before transferring the gas to the building exhaust stack. A catalytic reactor converts tritium gas (HT) to HTO prior to the molecular sieve stage. The molecular sieves are automatically regenerated *in situ*. Three molecular sieve beds are installed, allowing for continuous availability even during regeneration cycles. Input and output tritium and moisture monitors verify performance of the removal system and support a predictive maintenance plan that ensures high reliability and availability. To date, bed regenerations have yielded ~80 liters of tritiated water condensate containing 6 Ci of activity. The TC-TRS traps tritium in the exhaust from mechanical vacuum pumps used on the OMEGA target chamber.

The TC-TRS also receives effluent from the tritium scrubber. This is a small system that is dedicated to removing concentrated elemental tritium in the effluent from OMEGA cryogenic vacuum-pump regenerations. Most of the tritium released into the target chamber is collected by these pumps. The tritium scrubber employs zirconium-iron at elevated temperatures to reversibly adsorb elemental tritium. Effluent from the scrubber is then polished by the TC-TRS to remove residual tritium.

The target chamber's vacuum system and the auxiliary vacuum systems (e.g., for the ten-inch manipulators and the target positioner) have been modified to support decontamination cycles of the target chamber and antechambers. Modifications include the addition of purge-gas intake valves; a direct, atmospheric pressure path to the TC-TRS; and software and operating procedures to support automated decontamination of the target chamber and its antechambers. This operating mode makes it possible for equipment that has been exposed to tritium in the target chamber's vacuum envelope to be safely serviced, while minimizing personnel exposure to tritium and preventing contamination of the Target Bay environment.

The TC-TRS also receives effluent from Moving Cryostat Transfer Carts (MCTC's) as the result of decontamination activities in the Cart Maintenance Room. MCTC's are subjected to vent/pump cycles using room air to remove tritium from internal spaces. Effluent from the pump-out portion of the cycle is directed to the TC-TRS. Approximately 100 cycles are required over a period of two days to reduce concentrations to acceptable maintenance levels. Highly contaminated MCTC's have been observed to yield as much as 500 mCi during the decontamination process.

The TC-TRS modification makes it possible for OMEGA to shoot high-activity DT targets while providing a high degree of personnel safety and ensuring minimal release of tritium to the environment.

### **2.3.7 Software Improvements for OMEGA Operations**

OMEGA operations are supported by an array of software and database applications that capture the principal investigator's (PI's) shot specifications, categorize shots by their impact on the operational configuration, orchestrate the shot itself, collect and archive shot data, and provide data reduction for initial assessments. This system includes executive-level programs that communicate on an internal computer network and coordinate the activities of all shot-related programs. For example, the "Shot Executive," which is at the top of the executive-level hierarchy and operated by the Shot Director, propagates messages that transition the entire laser system from one well-defined state to the next. As the shot approaches, a precision hardware timing system counts down, fires the laser, and triggers all diagnostics for data acquisition.

The software suite has evolved as new capabilities have been added to the OMEGA Laser System and as computer-aided setup and monitoring have been applied to existing elements. The software framework has been extended and improved to accommodate joint shots using OMEGA EP. Significant improvements have been realized in the areas of object-oriented design; intra-program communication facilities; code development that employs mature, industry-recognized libraries; and source code control. The OMEGA EP laser system employs the same operational concepts as used on OMEGA and benefits from the software maturity of the older system.

While the two systems use separate databases for configuration and shot-data archiving, a common shot-request system serves to link the databases for shot preparation and data retrieval. The same executive-level software modules are used in both systems so that the "look and feel" of functions, terminology, and the user interface are shared.

### 2.3.8 Support for External Users

More than 60% of OMEGA shots are currently assigned to outside users. The support for these users is virtually the same as for LLE users and is centered around shot scheduling and planning, the integration of user-developed diagnostics, and user access to shot data.

#### (a) *Shot Planning*

A yearly OMEGA schedule is formulated three months before the beginning of the fiscal year. This allows Principal Investigators (PI's) to prepare and submit experimental proposals to the Facility Advisory and Scheduling Committee (FASC) for approval three months in advance of the experiment. Target requests are typically made to the target support contractor (GA) four months in advance of the planned experiments.

Subsequently, communicating the detailed requirements and specifications is accomplished through an automated shot request form (SRF) prepared by the PI for each shot. Video conferences or face-to-face meetings between LLE Operations Group leaders and external users are required both two weeks and one week prior to a campaign to review the SRF's. This ensures the accurate communication of user requirements and system capabilities.

#### (b) *Support for User-Developed Equipment*

A large number of instruments developed by external users have been deployed successfully on OMEGA. To permit the efficient integration of these subsystems, LLE provides standardized logistical support, a well-defined and reviewed entry and integration path, and extensive local support. Logistical support for external-user-developed diagnostics includes a standard interface into the target chamber, the ten-inch manipulator, or TIM, power and trigger feeds, a calibrated timing monitor system, and network connections and software interfaces to the OMEGA Control System. As necessary, on-site setup and calibration facilities are implemented to support diagnostics' operation developed by external users.

The smooth integration of instruments developed by external users is ensured by a uniform development/entry path for equipment being deployed on OMEGA. This procedure is governed by LLE Instruction 7700, which includes an Equipment Qualification Checklist (EQC), and supplements the developer's project management program. The EQC provides a series of waypoints and reviews with key LLE personnel to ensure that the new equipment will interface with OMEGA, will perform to required specifications, will not inhibit other system functions, and will not pose a safety hazard to personnel or other equipment on OMEGA.

The EQC procedure ensures readiness of the new equipment by disseminating vital information about the instrument's operation. This is accomplished through written procedures and documentation and by training operations personnel. Fit and function tests outlined by the EQC verify proper operation of the new equipment.

Frequently, the expertise of the external user's technical staff is critical to the operation of the user's equipment. It is necessary to provide the appropriate personnel facility qualification and training so that the users can operate and repair their equipment while it is installed on OMEGA. This program, designated Outside User's Training, ensures that the external user is aware of relevant safety and system issues prior to working in the Omega Facility environment.

(c) *Data Access*

Standard shot data (e.g., laser-performance information) are presented to the user in a package following each shot. Film records are available directly to the user.

Two means of accessing digital data are available. While on-site, the user may be issued an account that allows direct access to relevant data files. On- and off-site, the user may access authorized data files using a Web-based interface.

### 2.3.9 Operational Statistics

OMEGA capabilities, efficiency, and effectiveness have continued to improve, and OMEGA continues to be NNSA's principal laser facility for performing high-energy-density-physics experiments (Fig. 2.23).

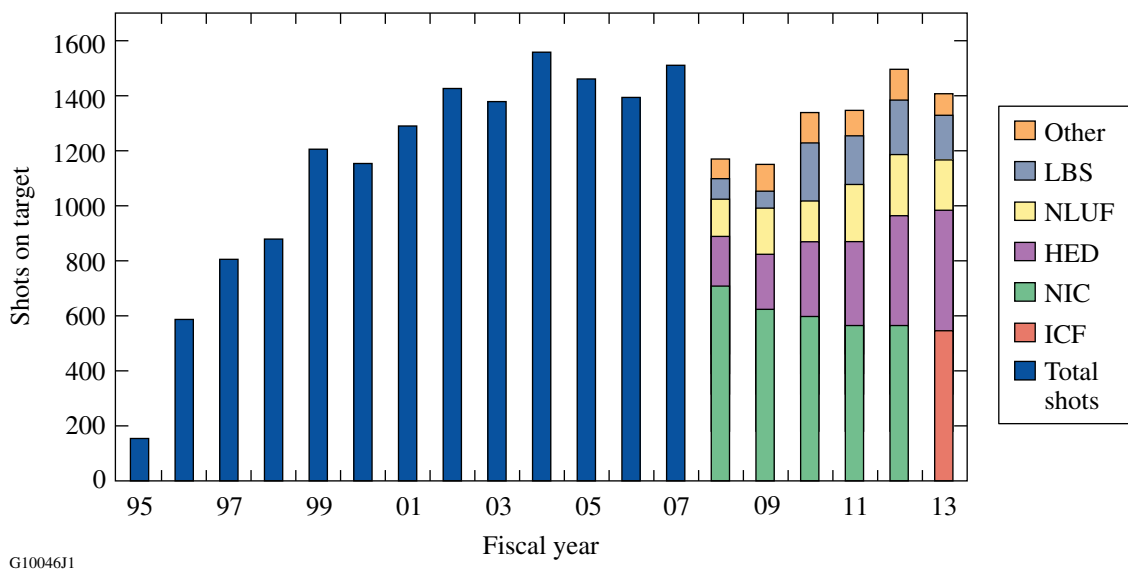


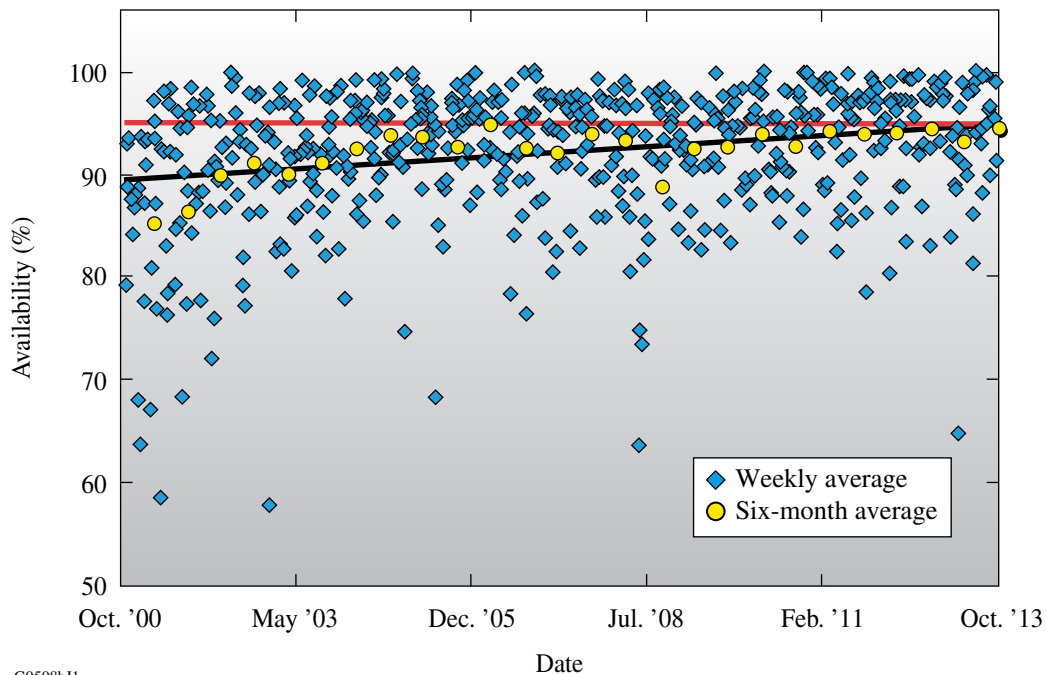
Figure 2.23  
OMEGA target shot production FY96 to FY13. (LBS: Laboratory Basic Science; NLUF: National Laser Users' Facility; HED: high-energy-density physics; NIC: National Ignition Campaign; ICF: inertial confinement fusion.)

OMEGA's reliability is measured by an availability statistic that quantifies the percentage of time that the system is ready for use during the scheduled operating hours. For the system availability to be 100%, the first daily target shot must occur by 9 AM with subsequent shots each hour thereafter. Each delay is categorized by subsystem and reason, and analysis is performed to identify operational and system improvements.

Figure 2.24 tracks the system availability over the past ten years. The trend in the six-month averages (yellow circles) indicates that the goal of 95% has been achieved.

OMEGA's experimental effectiveness is measured by the principal investigator evaluating the performance of the laser (energy, pulse shape, and timing), experimental diagnostics, and the target after each shot. The effectiveness of each shot is reviewed in real time to determine issues that require attention. Additionally, these statistics are analyzed to determine systematic issues to be addressed. Figure 2.25 tracks the experimental effectiveness over the past ten years. Again, the trend in the six-month averages indicates that the goal of 95% has been achieved.

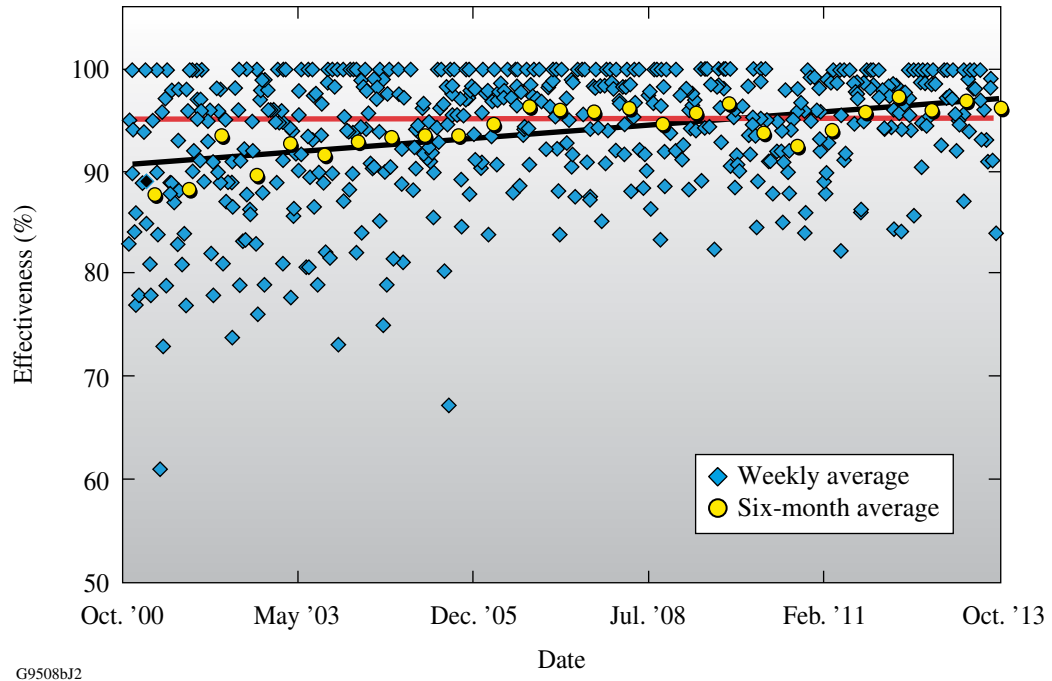
Overall, the statistics presented in this section illustrate that OMEGA operations are meeting the required shot schedules and setting a high standard for performance and reliability.



G9508bJ1

Figure 2.24

Average OMEGA system availability per shot week from October 2000 to September 2013. The yellow circles indicate averages over the previous six months and show progress toward the goal of 95% (red line).



G9508bJ2

Figure 2.25  
Average OMEGA experimental effectiveness per shot week from October 2000 to September 2013. The yellow circles indicate averages over the previous six months and show progress toward the goal of 95% (red line).

## 2.4 REFERENCES

1. "A Novel Energy Measurement System for the OMEGA Laser," *LLE Review Quarterly Report* **63**, 110, Laboratory for Laser Energetics, University of Rochester, Rochester, NY, LLE Document No. DOE/SF/19460-91, NTIS Order No. DE96000767 (1995).
2. T. J. Kessler, Y. Lin, J. J. Armstrong, and B. Velazquez, "Phase Conversion of Lasers with Low-Loss Distributed Phase Plates," in *Laser Coherence Control: Technology and Applications*, edited by H. T. Powell and T. J. Kessler (SPIE, Bellingham, WA, 1993), Vol. 1870, p. 95.
3. Y. Lin, T. J. Kessler, and G. N. Lawrence, "Design of Continuous Surface-Relief Phase Plates by Surface-Based Simulated Annealing to Achieve Control of Focal-Plane Irradiance," *Opt. Lett.* **21**, 1703 (1996).
4. T. J. Kessler, Y. Lin, L. S. Iwan, W. P. Castle, C. Kellogg, J. Barone, E. Kowaluk, A. W. Schmid, K. L. Marshall, D. J. Smith, A. L. Rigatti, J. Warner, and A. R. Staley, "Laser Phase Conversion Using Continuous Distributed Phase Plates," in *Second Annual International Conference on Solid State Lasers for Application to Inertial Confinement Fusion*, edited by M. L. André (SPIE, Bellingham, WA, 1997), Vol. 3047, p. 272.
5. S. Skupsky, R. W. Short, T. Kessler, R. S. Craxton, S. Letzring, and J. M. Soures, "Improved Laser-Beam Uniformity Using the Angular Dispersion of Frequency-Modulated Light," *J. Appl. Phys.* **66**, 3456 (1989).
6. S. Skupsky and R. S. Craxton, "Irradiation Uniformity for High-Compression Laser-Fusion Experiments," *Phys. Plasmas* **6**, 2157 (1999).
7. Y. Kato, K. Mima, N. Miyanaga, S. Arinaga, Y. Kitagawa, M. Nakatsuka, and C. Yamanaka, "Random Phasing of High-Power Lasers for Uniform Target Acceleration and Plasma-Instability Suppression," *Phys. Rev. Lett.* **53**, 1057 (1984).
8. "OMEGA Phase Conversion with Distributed Phase Plates," *LLE Review Quarterly Report* **33**, 1, Laboratory for Laser Energetics, University of Rochester, Rochester, NY, LLE Document No. DOE/DP/40200-65 (1987).
9. J. A. Menapace, S. N. Dixit, F. Y. Genin, and W. F. Brocious, "Magnetorheological Finishing for Imprinting Continuous-Phase Plate Structures onto Optical Surfaces," in *Laser-Induced Damage in Optical Materials: 2003*, edited by G. J. Exarhos, A. H. Guenther, N. Kaiser, K. L. Lewis, M. J. Soileau, and C. J. Stolz (SPIE, Bellingham, WA, 2003), Vol. 5273, p. 220.
10. H. G. Ahlstrom, "Lawrence Livermore National Laboratory Laser Fusion Program," Lawrence Livermore National Laboratory, Livermore, CA, UCRL-87114 (1982).

11. S. P. Regan, J. A. Marozas, J. H. Kelly, T. R. Boehly, W. R. Donaldson, P. A. Jaanimagi, R. L. Keck, T. J. Kessler, D. D. Meyerhofer, W. Seka, S. Skupsky, and V. A. Smalyuk, "Experimental Investigation of Smoothing by Spectral Dispersion," *J. Opt. Soc. Am. B* **17**, 1483 (2000).
12. S. P. Regan, J. A. Marozas, R. S. Craxton, J. H. Kelly, W. R. Donaldson, P. A. Jaanimagi, D. Jacobs-Perkins, R. L. Keck, T. J. Kessler, D. D. Meyerhofer, T. C. Sangster, W. Seka, V. A. Smalyuk, S. Skupsky, and J. D. Zuegel, "Performance of 1-THz-Bandwidth, Two-Dimensional Smoothing by Spectral Dispersion and Polarization Smoothing of High-Power, Solid-State Laser Beams," *J. Opt. Soc. Am. B* **22**, 998 (2005).
13. T. R. Boehly, V. A. Smalyuk, D. D. Meyerhofer, J. P. Knauer, D. K. Bradley, R. S. Craxton, M. J. Guardalben, S. Skupsky, and T. J. Kessler, "Reduction of Laser Imprinting Using Polarization Smoothing on a Solid-State Fusion Laser," *J. Appl. Phys.* **85**, 3444 (1999).
14. A. M. Cok, "Optimization of Polar-Direct-Drive Beam Profiles for Initial NIF Targets," *2007 Summer Research Program for High School Juniors at the University of Rochester's Laboratory for Laser Energetics*, University of Rochester, Rochester, NY (2008).
15. Zygo Mark IVxp<sup>TM</sup>, Zygo Corporation, Middlefield, CT 06455.
16. J. D. Moody, L. Divol, S. H. Glenzer, A. J. MacKinnon, D. H. Froula, G. Gregori, W. L. Kruer, L. J. Suter, E. A. Williams, R. Bahr, and W. Seka, "Experimental Studies of Simultaneous 351 nm and 527 nm Laser Beam Interactions in a Long Scalelength Plasma," in *Inertial Fusion Sciences and Applications 2003*, edited by B. A. Hammel, D. D. Meyerhofer, J. Meyer-ter-Vehn, and H. Azechi (American Nuclear Society, La Grange Park, IL, 2004), p. 218.
17. S. H. Glenzer, P. Arnold, G. Bardsley, R. L. Berger, G. Bonanno, T. Borger, D. E. Bower, M. Bowers, R. Bryant, S. Buckman, S. C. Burkhart, K. Campbell, M. P. Chrisp, B. I. Cohen, C. Constantin, F. Cooper, J. Cox, E. Dewald, L. Divol, S. Dixit, J. Duncan, D. Eder, J. Edwards, G. Erbert, B. Felker, J. Fornes, G. Frieders, D. H. Froula, S. D. Gardner, C. Gates, M. Gonzalez, S. Grace, G. Gregori, A. Greenwood, R. Griffith, T. Hall, B. A. Hammel, C. Haynam, G. Heestand, M. Henesian, G. Hermes, D. Hinkel, J. Holder, F. Holdner, G. Holtmeier, W. Hsing, S. Huber, T. James, S. Johnson, O. S. Jones, D. Kalantar, J. H. Kamperschroer, R. Kauffman, T. Kelleher, J. Knight, R. K. Kirkwood, W. L. Kruer, W. Labiak, O. L. Landen, A. B. Langdon, S. Langer, D. Latray, A. Lee, F. D. Lee, D. Lund, B. MacGowan, S. Marshall, J. McBride, T. McCarville, L. McGrew, A. J. Mackinnon, S. Mahavandi, K. Manes, C. Marshall, J. Menapace, E. Mertens, N. Meezan, G. Miller, S. Montelongo, J. D. Moody, E. Moses, D. Munro, J. Murray, J. Neumann, M. Newton, E. Ng, C. Niemann, A. Nikitin, P. Opsahl, E. Padilla, T. Parham, G. Parrish, C. Petty, M. Polk, C. Powell, I. Reinbachs, V. Rekow, R. Rinnert, B. Riordan, M. Rhodes, V. Roberts, H. Robey, G. Ross, S. Sailors, R. Saunders, M. Schmitt, M. B. Schneider, S. Shiromizu, M. Spaeth, A. Stephens, B. Still,

- L. J. Suter, G. Teitbohl, M. Tobin, J. Tuck, B. M. Van Wonterghem, R. Vidal, D. Voloshin, R. Wallace, P. Wegner, P. Whitman, E. A. Williams, K. Williams, K. Winward, K. Work, B. Young, P. E. Young, P. Zapata, R. E. Bahr, W. Seka, J. Fernandez, D. Montgomery, and H. Rose, "Progress in Long Scale Length Laser-Plasma Interactions," *Nucl. Fusion* **44**, S185 (2004).
18. C. Niemann, L. Divol, D. H. Froula, G. Gregori, O. Jones, R. K. Kirkwood, A. J. MacKinnon, N. B. Meezan, J. D. Moody, C. Sorce, L. J. Suter, R. Bahr, W. Seka, and S. H. Glenzer, "Intensity Limits for Propagation of  $0.527\ \mu\text{m}$  Laser Beams Through Large-Scale-Length Plasmas for Inertial Confinement Fusion," *Phys. Rev. Lett.* **94**, 085005 (2005).
  19. D. H. Froula, P. Davis, L. Divol, J. S. Ross, N. Meezan, D. Price, S. H. Glenzer, and C. Rousseaux, "Measurement of the Dispersion of Thermal Ion-Acoustic Fluctuations in High-Temperature Laser Plasmas Using Multiple-Wavelength Thomson Scattering," *Phys. Rev. Lett.* **95**, 195005 (2005).
  20. S. H. Glenzer, D. H. Froula, S. Ross, C. Niemann, N. Meezan, and L. Divol, "Characterization of High-Temperature Laser-Produced Plasmas Using Thomson Scattering," Lawrence Livermore National Laboratory, Livermore, CA, UCRL-PROC-215698 (2005).
  21. W. R. Donaldson, M. Millecchia, and R. Keck, "A Multichannel, High-Resolution, UV Spectrometer for Laser-Fusion Applications," *Rev. Sci. Instrum.* **76**, 073106 (2005).
  22. R. S. Craxton, "High Efficiency Frequency Tripling Schemes for High Power Nd:Glass Lasers," *IEEE J. Quantum Electron.* **QE-17**, 1771 (1981).
  23. D. Eimerl, J. M. Auerbach, C. E. Barker, D. Milam, and P. W. Milonni, "Multicrystal Designs for Efficient Third-Harmonic Generation," *Opt. Lett.* **22**, 1208 (1997).
  24. A. Babushkin, R. S. Craxton, S. Oskoui, M. J. Guardalben, R. L. Keck, and W. Seka, "Demonstration of the Dual-Tripler Scheme for Increased-Bandwidth Third-Harmonic Generation," *Opt. Lett.* **23**, 927 (1998).
  25. Y. R. Shen, *The Principles of Nonlinear Optics* (Wiley, New York, 1984), p. 324.
  26. R. Kekre, "Tuning Multiple Triplers Using a UV Spectrometer," *2003 Summer Research Program for High School Juniors at the University of Rochester's Laboratory for Laser Energetics*, University of Rochester, Rochester, NY, LLE Report No. 332, LLE Document No. DOE/SF19460-526 (2004).